Guiding center motion in tokamaks

BY YOUJUN HU

Institute of plasma physics, Chinese Academy of Sciences
Email: yjhu@ipp.cas.cn

Abstract

This note discusses numerical computation of guiding center orbits in tokamaks using cylindrical coordinates and several magnetic coordinates. Some subtle things involved in using a particular kind of magnetic coordinates called field-line-following coordinates are discussed (I am using this kind of coordinates in developing a new module in GEM code). We assume a general tokamak magnetic field specified numerically (provided by the EFIT G-file). This note is evolving, beginning with my first try of computing guiding-center motion in Solovev analytical equilibrium using cylindrical coordinates, and then extending to general numerical magnetic field, and later using magnetic coordinates.

1 Equations of guiding-center motion

The equations of guiding center motion are given by[1]

$$\frac{d\mathbf{X}}{dt}=\frac{\mathbf{B}^\star}{B_\parallel^\star}v_\parallel+\frac{\mu}{m\Omega B_\parallel^\star}\mathbf{B}\times\nabla B+\frac{1}{BB_\parallel^\star}\mathbf{E}\times\mathbf{B} \tag{1}$$

$$\frac{dv_\parallel}{dt}=-\frac{\mu}{m}\frac{\mathbf{B}^\star}{B_\parallel^\star}\cdot\nabla B+\frac{Ze}{m}\frac{\mathbf{B}^\star}{B_\parallel^\star}\cdot\mathbf{E} \tag{2}$$

where $\mathbf{X}$ is the guiding-center position, $v_\parallel$ is the parallel (to the magnetic field) velocity defined by $v_\parallel=\mathbf{B}\cdot\mathbf{v}/B$; Here m, Ze, and $\mathbf{v}$ are the mass, charge and velocity of the particle, respectively, μ is the magnetic moment defined by $\mu=mv_\perp^2/(2B)$ with $v_\perp$ being the perpendicular speed; $\Omega=BZe/m$ is the cyclotron angular frequency, $\mathbf{B}^\star$ and $B_\parallel^\star$ are defined by

$$\mathbf{B}^\star=\mathbf{B}+B\frac{v_\parallel}{\Omega}\nabla\times\mathbf{b}, \tag{3}$$

$$B_\parallel^\star\equiv\mathbf{b}\cdot\mathbf{B}^\star=B\Big(1+\frac{v_\parallel}{\Omega}\mathbf{b}\cdot\nabla\times\mathbf{b}\Big), \tag{4}$$

respectively, where $\mathbf{b}=\mathbf{B}/B$. If we use the approximation $B_\parallel^\star\approx B$, then the drift velocity in Eq. (1) can be written as

$$\frac{d\mathbf{X}}{dt}=v_\parallel\mathbf{e}_\parallel+\mathbf{V}_D=v_\parallel\mathbf{b}+\underbrace{\frac{v_\parallel^2}{\Omega}\nabla\times\mathbf{b}}_{\text{curvaturedrift}}+\underbrace{\frac{\mu}{m\Omega B}\mathbf{B}\times\nabla B_0}_{\nabla B\text{drift}}+\underbrace{\frac{1}{B^2}\mathbf{E}\times\mathbf{B}}_{E\times B\text{drift}}, \tag{5}$$

where the usual drifts can be recognized. Before getting to know the above form of the equations of the guiding-center motion, I used the following form of the equations (refer to my notes "collisionless_drift_kinetic_equation.tm"):

$$\frac{d\mathbf{X}}{dt}=\mathbf{b}v_\parallel+\frac{1}{\Omega}\mathbf{b}\times\left(\frac{\mu}{m}\nabla B+v_\parallel^2\boldsymbol{\kappa}-\frac{Ze}{m}\mathbf{E}\right), \tag{6}$$

$$\frac{dv_\parallel}{dt}=-\frac{\mu}{m}\mathbf{b}\cdot\nabla B+\frac{v_\parallel\mu}{m\Omega}\boldsymbol{\kappa}\cdot\mathbf{b}\times\nabla B+\frac{Ze}{m}\mathbf{b}\cdot\mathbf{E}, \tag{7}$$

which does not conserve the toroidal angular momentum P_ϕ exactly in an axisymmetrical equilibrium magnetic field (this has been tested numerically) while the new form given in Eqs. (1)-(4) can conserve P_ϕ exactly. My latest numerical code uses Eqs. (1)-(4) as the the equations of guiding center motion. The toroidal angular momentum P_ϕ is defined by

$$P_\phi=m\frac{g(\Psi)}{B}v_\parallel+Ze\Psi, \tag{8}$$

where $\Psi=A_\phi R$ with A_ϕ being the toroidal component of the magnetic vector potential.

1.1 Define new units

The above formulas are in SI units, which are good since SI units are widely used and thus these formulas are accessible to most people, making communications easier. However, many physicists prefer to define new units for a specific problem and write the equations in terms of these new units. This process is often called normalization. This has the advantage of possibly reducing the number of free parameters in a problem. Another advantage is that, by chosen proper characteristic quantities as units, the magnitude of quantities in terms of the new units are easier to be appreciated. A third advantage is that the magnitude of normalized quantities may be in the vicinity of 1 (if suitable units are chosen), and thus numerical overflow in a numerical computation may be avoided, making the computation more accurate. The disadvantages of the normalization are (1) the additional work associated with performing the transformation between two units systems, (2) possible confusions about which units are used in a numerical code and the potential of introducing bugs due to this confusion when writing or revising numerical codes.

The units I adopted are as follows. Choose a characteristic magnetic field strength B_n and a characteristic length L_n. Using B_n and L_n, we define a characteristic time $t_n \equiv 2\pi / \Omega_n$, where $\Omega_n = B_n|Ze|/m$, a characteristic velocity $v_n = L_n / t_n$, and a characteristic magnetic moment $\mu_n = m v_n^2 / B_n$. Using these characteristic quantities as units, I define the following normalized quantities:

$$\overline{\mathbf{X}} = \frac{\mathbf{X}}{L_n}, \overline{\nabla} = L_n \nabla, \bar{t} = \frac{t}{t_n}, \bar{v}_\parallel = \frac{v_\parallel}{v_n}, \bar{\mu} = \frac{\mu}{\mu_n}, \overline{\mathbf{B}} = \frac{\mathbf{B}}{B_n}, \overline{\mathbf{B}^\star} = \frac{\mathbf{B}^\star}{B_n}, \overline{B_\parallel^\star} = \frac{B_\parallel^\star}{B_n}, \overline{\mathbf{E}} = \frac{\mathbf{E}}{B_n v_n}. \tag{9}$$

In terms of the above normalized quantities, Eqs. (1)-(4) are written, respectively, as

$$\frac{d\overline{\mathbf{X}}}{d\bar{t}} = \frac{\overline{\mathbf{B}^\star}}{\overline{B_\parallel^\star}} \bar{v}_\parallel + \frac{Z}{|Z|} \frac{\bar{\mu}}{2\pi \overline{B}\, \overline{B_\parallel^\star}} \overline{\mathbf{B}} \times \overline{\nabla} \overline{B} + \frac{1}{\overline{B}\, \overline{B_\parallel^\star}} \overline{\mathbf{E}} \times \overline{\mathbf{B}}, \tag{10}$$

$$\frac{d\bar{v}_\parallel}{d\bar{t}} = -\bar{\mu} \frac{\overline{\mathbf{B}^\star}}{\overline{B_\parallel^\star}} \cdot \overline{\nabla} \overline{B} + \frac{Z}{|Z|} 2\pi \frac{\mathbf{B}^\star}{B_\parallel^\star} \cdot \overline{\mathbf{E}}, \tag{11}$$

$$\overline{\mathbf{B}^\star} = \overline{\mathbf{B}} + \frac{Z}{|Z|} \frac{\bar{v}_\parallel}{2\pi} \overline{\nabla} \times \mathbf{b}, \tag{12}$$

and

$$\overline{B_\parallel^\star} = \overline{B} + \frac{Z}{|Z|} \frac{\bar{v}_\parallel}{2\pi} \mathbf{b} \cdot \overline{\nabla} \times \mathbf{b}. \tag{13}$$

In the normalized form, there is only one parameter for distinguishing particle species, namely the sign of particle's charge $Z/|Z|$. The other parameters for particle species enters via the normalization factor $\Omega_n = B_n|Ze|/m$.

The toroidal angular momentum P_ϕ is normalized by $Ze B_n L_n^2$.

In TEK code, I choose $B_n = 1T$ and $L_n = 1m$, i.e., they are identical to the corresponding SI units. This choice makes my unit system become bad because it is hard to relate v_n defined above to any typical velocity in a tokamak plasma. A better choice would be choose B_n to the magnetic field magnitude at the magnetic axis and choose L_n to be v_t / Ω_n, i.e., the Larmor radius of a typical particles, where v_t is the thermal velocity of a species. Then define $t_n = 1/\Omega_n$ and define v_n by $v_n = L_n / t_n = v_t$, which is a typical particle velocity. In future, I may change TEK code to using this unit system, but presently I stick to using the above unit system.

2 Equation of guiding-center motion in field-line-following coordinates

Consider the field-line-following coordinates (ψ, θ, α), where α is the generalized toroidal angle defined by $\alpha = \phi - \bar{\delta}$ with $\bar{\delta} = \int_0^\theta \hat{q} d\theta$ and $\hat{q} = \mathbf{B} \cdot \nabla \phi / (\mathbf{B} \cdot \nabla \theta)$, which is the local safety factor. The time evolution of (ψ, θ, α) of a guiding-center is then written as

$$\frac{d\psi}{d\bar{t}} = \frac{\partial \psi}{\partial \bar{t}} + \frac{d\overline{\mathbf{X}}}{d\bar{t}} \cdot \overline{\nabla} \psi = \frac{d\overline{\mathbf{X}}}{d\bar{t}} \cdot \overline{\nabla} \psi, \tag{14}$$

and similarly

$$\frac{d\,\theta}{d\,\bar{t}} = \frac{d\overline{\mathbf{X}}}{d\bar{t}} \cdot \overline{\nabla}\,\theta, \tag{15}$$

$$\frac{d\,\alpha}{d\,\bar{t}} = \frac{d\overline{\mathbf{X}}}{d\bar{t}} \cdot \overline{\nabla}\,\alpha, \tag{16}$$

Using the expression of $d\overline{\mathbf{X}}\,/\,dt$ given by Eq. (10), Eqs. (14)-(16) can be written as (presently dropping the $\mathbf{E}\times\mathbf{B}$ drift, which will be discussed later):

$$\frac{d\,\psi}{d\,\bar{t}} = \bar{v}_{\parallel}\frac{\frac{Z}{|Z|}\frac{\bar{v}_{\parallel}}{2\pi}\overline{\nabla}\times\mathbf{b}}{\overline{B}\left(1+\frac{Z}{|Z|}\frac{\bar{v}_{\parallel}}{2\pi\overline{B}}\mathbf{b}\cdot\overline{\nabla}\times\mathbf{b}\right)}\cdot\overline{\nabla}\ \psi + \frac{Z}{|Z|}\frac{\bar{\mu}}{2\pi\left(1+\frac{Z}{|Z|}\frac{\bar{v}_{\parallel}}{2\pi\overline{B}}\mathbf{b}\cdot\overline{\nabla}\times\mathbf{b}\right)}\frac{1}{\overline{B}^2}\overline{\mathbf{B}}\ \times\ \overline{\nabla}\overline{B}\ \cdot\ \overline{\nabla}\ \psi, \tag{17}$$

$$\frac{d\,\theta}{d\,\bar{t}} = \bar{v}_{\parallel}\frac{\overline{\mathbf{B}}+\frac{Z}{|Z|}\frac{\bar{v}_{\parallel}}{2\pi}\overline{\nabla}\times\mathbf{b}}{\overline{B}\left(1+\frac{Z}{|Z|}\frac{\bar{v}_{\parallel}}{2\pi\overline{B}}\mathbf{b}\cdot\overline{\nabla}\times\mathbf{b}\right)}\cdot\overline{\nabla}\,\theta + \frac{Z}{|Z|}\frac{\bar{\mu}}{2\pi\left(1+\frac{Z}{|Z|}\frac{\bar{v}_{\parallel}}{2\pi\overline{B}}\mathbf{b}\cdot\overline{\nabla}\times\mathbf{b}\right)}\frac{1}{\overline{B}^2}\overline{\mathbf{B}}\times\overline{\nabla}\overline{B}\cdot\overline{\nabla}\,\theta, \tag{18}$$

$$\frac{d\,\alpha}{d\,\bar{t}} = \bar{v}_{\parallel}\frac{\frac{Z}{|Z|}\frac{\bar{v}_{\parallel}}{2\pi}\overline{\nabla}\times\mathbf{b}}{\overline{B}\left(1+\frac{Z}{|Z|}\frac{\bar{v}_{\parallel}}{2\pi\overline{B}}\mathbf{b}\cdot\overline{\nabla}\times\mathbf{b}\right)}\cdot\overline{\nabla}\,\alpha + \frac{Z}{|Z|}\frac{\bar{\mu}}{2\pi\left(1+\frac{Z}{|Z|}\frac{\bar{v}_{\parallel}}{2\pi\overline{B}}\mathbf{b}\cdot\overline{\nabla}\times\mathbf{b}\right)}\frac{1}{\overline{B}^2}\overline{\mathbf{B}}\times\overline{\nabla}\overline{B}\cdot\overline{\nabla}\,\alpha. \tag{19}$$

where use has been made of $\mathbf{B}\cdot\nabla\psi = 0$ and $\mathbf{B}\cdot\nabla\alpha = 0$. The parallel acceleration equation is written as (presently dropping the electric field acceleration term)

$$\frac{d\,\bar{v}_{\parallel}}{d\,\bar{t}} = -\bar{\mu}\frac{\overline{\mathbf{B}}+\frac{Z}{|Z|}\frac{\bar{v}_{\parallel}}{2\pi}\overline{\nabla}\times\mathbf{b}}{\overline{B}\left(1+\frac{Z}{|Z|}\frac{\bar{v}_{\parallel}}{2\pi\overline{B}}\mathbf{b}\cdot\overline{\nabla}\times\mathbf{b}\right)}\cdot\overline{\nabla}\overline{B} \tag{20}$$

For a general tokamak magnetic configuration specified numerically, all the above 2D equilibrium quantities are computed by interpolating pre-computed numerical tables. We define the following numerical tables:

$$W_1(\psi,\theta) = \frac{1}{\overline{B}}\mathbf{b}\cdot\overline{\nabla}\times\mathbf{b}, \tag{21}$$

$$W_2(\psi,\theta) = \frac{\overline{\mathbf{B}}}{\overline{B}}\cdot\overline{\nabla}\,\theta, \tag{22}$$

$$W_3(\psi,\theta) = \frac{\overline{\nabla}\times\mathbf{b}}{\overline{B}}\cdot\overline{\nabla}\,\psi, \tag{23}$$

$$W_4(\psi,\theta) = \frac{\overline{\nabla}\times\mathbf{b}}{\overline{B}}\cdot\overline{\nabla}\,\theta, \tag{24}$$

$$W_5(\psi,\theta,\alpha) = \frac{\overline{\nabla}\times\mathbf{b}}{\overline{B}}\cdot\overline{\nabla}\,\alpha = \frac{\overline{\nabla}\times\mathbf{b}}{\overline{B}}\cdot\overline{\nabla}\,\phi - \frac{\overline{\nabla}\times\mathbf{b}}{\overline{B}}\cdot\overline{\nabla}\bar{\delta} \tag{25}$$

$$W_6(\psi,\theta) = \frac{1}{\overline{B}^2}\overline{\mathbf{B}}\times\overline{\nabla}\overline{B}\cdot\overline{\nabla}\,\psi, \tag{26}$$

$$W_7(\psi,\theta) = \frac{1}{\overline{B}^2}\overline{\mathbf{B}}\times\overline{\nabla}\overline{B}\cdot\overline{\nabla}\,\theta, \tag{27}$$

$$W_8(\psi,\theta,\alpha) = \frac{1}{\overline{B}^2}\overline{\mathbf{B}}\times\overline{\nabla}\overline{B}\cdot\overline{\nabla}\,\alpha = \frac{1}{\overline{B}^2}\overline{\mathbf{B}}\times\overline{\nabla}\overline{B}\cdot\overline{\nabla}\,\phi - \frac{1}{\overline{B}^2}\overline{\mathbf{B}}\times\overline{\nabla}\overline{B}\cdot\overline{\nabla}\bar{\delta} \tag{28}$$

$$W_9(\psi,\theta) = \frac{\overline{\mathbf{B}}}{\overline{B}}\cdot\overline{\nabla}\overline{B}, \tag{29}$$

$$W_{10}(\psi,\theta) = \frac{\overline{\nabla}\times\mathbf{b}}{\overline{B}}\cdot\overline{\nabla}\,\overline{B}. \tag{30}$$

Next, let us discuss the $\mathbf{E}\times\mathbf{B}$ drift:

$$\overline{\mathbf{v}}_{E\times B}\cdot\nabla\psi = \frac{1}{\overline{B}\,\overline{B}^{\star}_{\parallel}}\overline{\mathbf{E}}\times\overline{\mathbf{B}}\cdot\overline{\nabla}\,\psi \tag{31}$$

$$\overline{\mathbf{v}}_{E\times B}\cdot\nabla\theta = \frac{1}{\overline{B}\,\overline{B}^{\star}_{\parallel}}\overline{\mathbf{E}}\times\overline{\mathbf{B}}\cdot\overline{\nabla}\,\theta \tag{32}$$

$$\overline{\mathbf{v}}_{E\times B}\cdot\nabla\alpha = \frac{1}{\overline{B}\,\overline{B}^{\star}_{\parallel}}\overline{\mathbf{E}}\times\overline{\mathbf{B}}\cdot\overline{\nabla}\,\alpha \tag{33}$$

Using $\delta\overline{\mathbf{E}} = \delta\overline{E}_{\parallel}\mathbf{b} + \delta\overline{E}_x\overline{\nabla}x + \delta\overline{E}_y\overline{\nabla}y$, where $x=\psi$ and $y=\alpha$, the above drifts are written as

$$\begin{aligned}
\overline{\mathbf{v}}_{E\times B}\cdot\nabla x &= \frac{1}{\overline{B}\,\overline{B}^{\star}_{\parallel}}(\delta\overline{E}_x\overline{\nabla}x + \delta\overline{E}_y\overline{\nabla}y)\times\overline{\mathbf{B}}\cdot\overline{\nabla}\,x \\
&= -\frac{1}{\overline{B}\,\overline{B}^{\star}_{\parallel}}(\delta\overline{E}_x\overline{\nabla}x + \delta\overline{E}_y\overline{\nabla}y)\times\overline{\nabla}\,x\cdot\overline{\mathbf{B}} \\
&= -\frac{1}{\overline{B}\,\overline{B}^{\star}_{\parallel}}(\delta\overline{E}_y\overline{\nabla}y)\times\overline{\nabla}\,x\cdot\overline{\mathbf{B}} \\
&= \frac{1}{\overline{B}\,\overline{B}^{\star}_{\parallel}}(\delta\overline{E}_y)\overline{\nabla}x\times\overline{\nabla}\,y\cdot\overline{\mathbf{B}} \\
&= \frac{1}{\overline{B}\,\overline{B}^{\star}_{\parallel}}(\delta\overline{E}_y)\frac{\overline{\mathbf{B}}}{\overline{\Psi}'}\cdot\overline{\mathbf{B}}
\end{aligned} \tag{34}$$

$$\begin{aligned}
\overline{\mathbf{v}}_{E\times B}\cdot\nabla y &= \frac{1}{\overline{B}\,\overline{B}^{\star}_{\parallel}}(\delta\overline{E}_x\overline{\nabla}x + \delta\overline{E}_y\overline{\nabla}y)\times\overline{\mathbf{B}}\cdot\overline{\nabla}\,y \\
&= -\frac{1}{\overline{B}\,\overline{B}^{\star}_{\parallel}}(\delta\overline{E}_x\overline{\nabla}x + \delta\overline{E}_y\overline{\nabla}y)\times\overline{\nabla}\,y\cdot\overline{\mathbf{B}} \\
&= -\frac{1}{\overline{B}\,\overline{B}^{\star}_{\parallel}}(\delta\overline{E}_x\overline{\nabla}x)\times\overline{\nabla}\,y\cdot\overline{\mathbf{B}} \\
&= -\frac{1}{\overline{B}\,\overline{B}^{\star}_{\parallel}}(\delta\overline{E}_x)\frac{\overline{\mathbf{B}}}{\overline{\Psi}'}\cdot\overline{\mathbf{B}}
\end{aligned} \tag{35}$$

$$\begin{aligned}
\overline{\mathbf{v}}_{E\times B}\cdot\nabla\theta &= \frac{1}{\overline{B}\,\overline{B}^{\star}_{\parallel}}(\delta\overline{E}_x\overline{\nabla}\psi + \delta\overline{E}_y\overline{\nabla}\alpha)\times\overline{\mathbf{B}}\cdot\overline{\nabla}\,\theta \\
&= -\frac{1}{\overline{B}\,\overline{B}^{\star}_{\parallel}}(\delta\overline{E}_x\overline{\mathbf{B}}\cdot\overline{\nabla}\psi\times\overline{\nabla}\,\theta + \delta\overline{E}_y\overline{\mathbf{B}}\cdot\overline{\nabla}\alpha\times\overline{\nabla}\,\theta).
\end{aligned} \tag{36}$$

The two terms in expression (36) can be written as

$$\begin{aligned}
\overline{\mathbf{B}}\cdot(\overline{\nabla}\psi\times\overline{\nabla}\,\theta) &= \overline{\mathbf{B}}\cdot\begin{vmatrix} \mathbf{e}_R & \mathbf{e}_\phi & \mathbf{e}_Z \\ \frac{\partial\psi}{\partial R} & 0 & \frac{\partial\psi}{\partial Z} \\ \frac{\partial\theta}{\partial R} & 0 & \frac{\partial\theta}{\partial Z} \end{vmatrix} \\
&= \overline{B}_\phi\left(\frac{\partial\psi}{\partial Z}\frac{\partial\theta}{\partial R} - \frac{\partial\psi}{\partial R}\frac{\partial\theta}{\partial Z}\right) \\
&\equiv W_{14}
\end{aligned}$$

$$\begin{aligned}\overline{\mathbf{B}}\cdot(\overline{\nabla}\alpha\times\overline{\nabla}\,\theta) &= \overline{\mathbf{B}}\cdot\begin{vmatrix}\mathbf{e}_R & \mathbf{e}_\phi & \mathbf{e}_Z\\ \frac{\partial\alpha}{\partial R} & \frac{1}{R}\frac{\partial\alpha}{\partial\phi} & \frac{\partial\alpha}{\partial Z}\\ \frac{\partial\theta}{\partial R} & 0 & \frac{\partial\theta}{\partial Z}\end{vmatrix}\\ &= \overline{B}_R\left(\frac{1}{R}\frac{\partial\alpha}{\partial\phi}\frac{\partial\theta}{\partial Z}\right)+\overline{B}_\phi\left(\frac{\partial\alpha}{\partial Z}\frac{\partial\theta}{\partial R}-\frac{\partial\alpha}{\partial R}\frac{\partial\theta}{\partial Z}\right)+\overline{B}_Z\left(-\frac{1}{R}\frac{\partial\alpha}{\partial\phi}\frac{\partial\theta}{\partial R}\right)\\ &\equiv W_{15}\end{aligned}$$

2.0.1 Periodic conditions of particle trajectory in field-line-following coordinates

Note that $\theta(\mathbf{r})$ and $\phi(\mathbf{r})$ are multi-valued functions whereas $\nabla\theta(\mathbf{r})$ and $\nabla\phi(\mathbf{r})$ happen to be single-valued functions. However $\nabla\alpha(\mathbf{r})$ and $\nabla\bar{\delta}(\mathbf{r})$ are still multi-valued functions. [It is ready to see this by examining the special case that θ is a straight-field line poloidal angle, in which $\bar{\delta}=\int_{\theta_{\rm ref}}^{\theta}\hat{q}d\theta$ is simplified to $q\theta$. Then $\nabla\bar{\delta}$ is written as

$$\nabla\bar{\delta}=\theta\nabla q+q\nabla\theta, \tag{37}$$

where the first term $\theta\nabla q$ is a multi-valued function since θ is multi-valued.]

For multi-valued functions, if a single branch is chosen, then there will be discontinuity at the the branch cut. In numerically constructing the coordinates (ψ,θ,α), the principal value of θ is chosen in the range $[-\pi\text{: }\pi)$ and the branch cut for θ is chosen on the high-field-side mid-plane. The toroidal shift $\bar{\delta}=\int_{\theta_{\rm ref}}^{\theta}\hat{q}\,d\,\theta$ can be considered as a derived angle based on θ and thus its principal value and branch cut are determined by those of θ.

The (ψ, θ, α) coordinates of a particle change continuously when we evolve them by integrating Eqs. (14)-(16), during which θ can move beyond $[-\pi,\,\pi)$. When a particle's θ moves beyond the range $[-\pi\text{: }\pi)$, one or multiple $\pm2\pi$ shifts are imposed on θ until θ are within $[-\pi\text{: }\pi)$. Note that a corresponding shift in α is needed to keep the particle at the same spatial location when doing the θ shift. This is because, although (ψ,θ,ϕ) and $(\psi,\theta-2m\pi,\phi)$ correspond to the same spatial location, points (ψ,θ,α) and $(\psi,\theta-2m\pi,\alpha)$ do not, where m is an integer. Specifically, the usual toroidal angle ϕ of point (ψ,θ,α) is $\phi_1=\alpha+\int_{\theta_{\rm ref}}^{\theta}\hat{q}d\theta$ while ϕ of point (ψ, $\theta-2m\pi,\alpha)$ is $\phi_2=\alpha+\int_{\theta_{\rm ref}}^{\theta-2m\pi}\hat{q}d\theta$. The difference between ϕ_1 and ϕ_2 is $\phi_2-\phi_1=-2m\pi q$. This indicates that, to keep the point at the same spatial location when shifting θ by $-2m\pi$, α should be shifted by $+2m\pi q$, i.e., the new coordinates of the point should be $(\psi,\theta-2m\pi,\alpha+2m\pi q)$. This process is illustrated in Fig. 1. A typical evolution of $(\theta,\,\alpha)$ involving shifting is shown in Fig. 2.

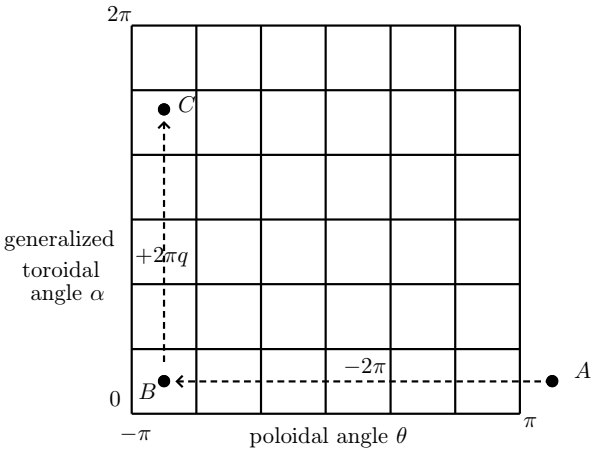

Figure 1. To keep the point at the same spatial location when shifting θ by -2π, α should be shifted by $+2\pi q$. Here A and C correspond to the same spatial location, but B is at a different location.

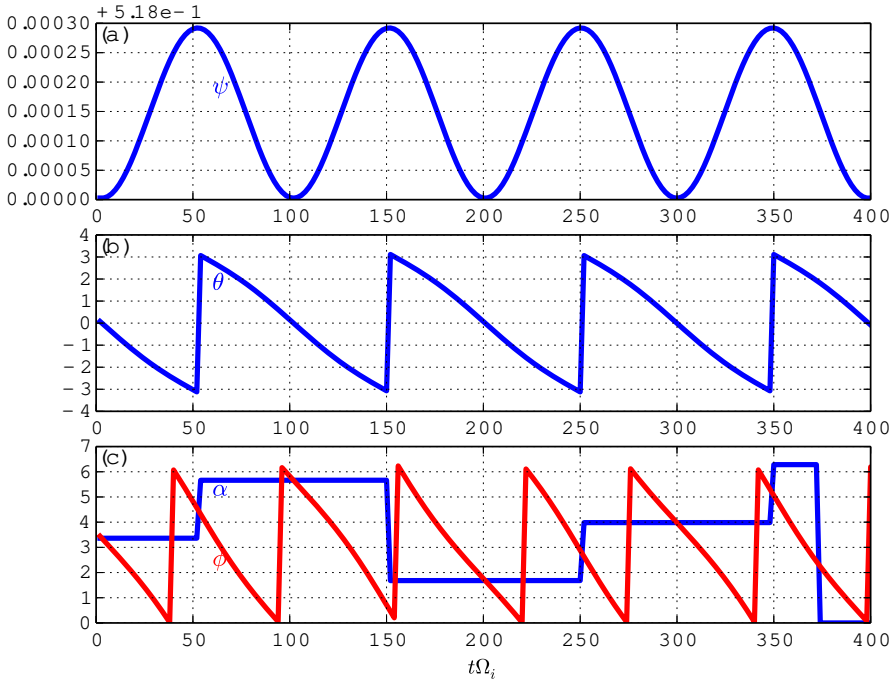

Figure 2. Temporal evolution of (ψ, θ, α) of a passing electron. The range of θ is chosen to be $[-\pi\colon \pi]$ and the range of α and ϕ is $[0\colon 2\pi]$. When θ exceed the range, a 2π shift is imposed, which generate the jump of θ in (b) and also the corresponding jump of α in (c). Note that when a jump in (θ, α) occurs, no jump in ϕ, which is what we expect, otherwise there must be something wrong. Also note that there are also jumps of ϕ shown in (c), which is due to ϕ exceeding the range $[0\colon 2\pi]$ and a 2π shift being imposed. This jump has nothing to do with the jump in θ or α and usually occur at different time (one jump of ϕ is near the jump of α, which is only a coincidence). Here ϕ is computed using $\phi = \alpha + \bar{\delta}$, where $\bar{\delta}$ is obtained by interpolating the 2D numerical table of $\bar{\delta}(\psi, \theta)$. DIID-D cyclone base case

When α exceeds the range $[0\colon 2\pi]$, one or multiple $\pm 2\pi$ shifts are imposed on α until α are within $[0\colon 2\pi]$. Since, for fixed ψ and θ, the generalized toroidal angle α is equivalent to the usual toroidal angle ϕ. No complication like the case of θ arises when doing the α shift.

One way of avoiding the subtle (θ, α) shift problem is to evolve particles' ϕ, instead of α. In this case, we have

$$\frac{d\,\phi}{d\,\bar{t}} = \bar{\mathbf{v}}_d \cdot \overline{\nabla}\,\phi \;=\; \bar{v}_{\parallel} \frac{\overline{\mathbf{B}} + \frac{\bar{v}_{\parallel}}{2\pi}\overline{\nabla}\times\mathbf{b}}{\overline{B}\left(1 + \frac{\bar{v}_{\parallel}}{2\pi\overline{B}}\mathbf{b}\cdot\overline{\nabla}\times\mathbf{b}\right)} \cdot \overline{\nabla}\,\phi + \frac{\bar{\mu}}{2\pi\left(1 + \frac{\bar{v}_{\parallel}}{2\pi\overline{B}}\mathbf{b}\cdot\overline{\nabla}\times\mathbf{b}\right)} \frac{1}{\overline{B}^2}\overline{\mathbf{B}}\times\overline{\nabla}\overline{B}\cdot\overline{\nabla}\,\phi, \qquad (38)$$

After getting ϕ, we use $\alpha = \phi - \bar{\delta}(\psi, \theta)$ to get particles' α, where $\bar{\delta}$ is obtained by interpolating the numerical table in $(\psi,\ \theta)$ plane. I have tested the two ways of computing evolution of α, which indicates their results agree with each other. In the final codes, I use the $(\theta,\ \alpha)$ shift method, because this methods involve less interpolation and thus more efficient.

2.0.2 Benchmarking cases

To verify code implementation, two methods are used to compute the guiding-center orbits. The first method uses the cylindrical coordinates and then interpolate the orbits into magnetic coordinates using pre-computed mapping table between the cylindrical and magnetic coordinates. The second method directly uses the magnetic coordinates in pushing the orbits. The following figures compare the results obtained by these two methods, which indicates they agree with each other. This provides confidence on the correctness of the numerical implementation.

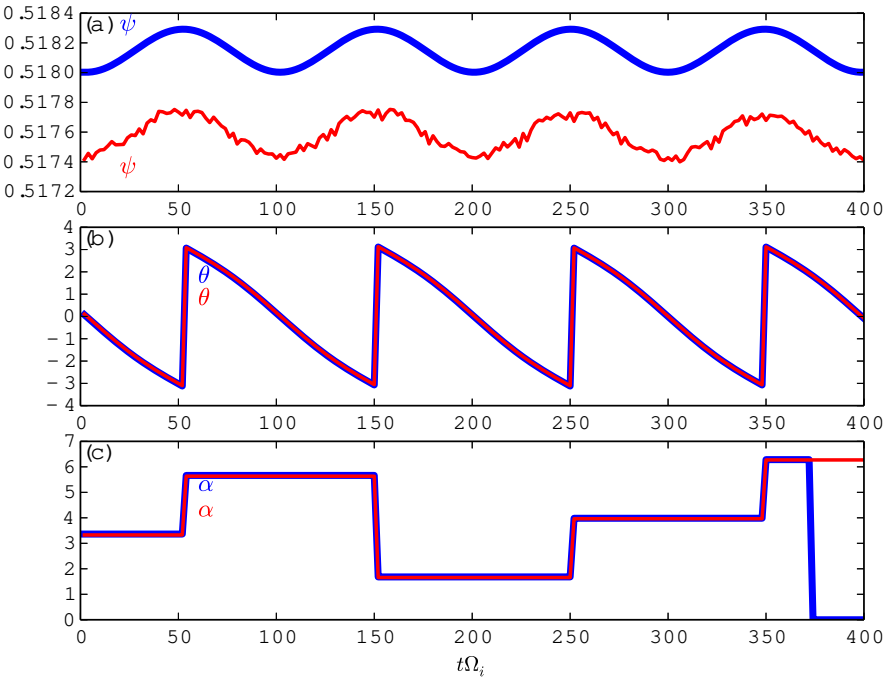

Figure 3. Comparison between the temporal evolution of (ψ, θ, α) of a passing electron computed by two methods: the blue lines are the results computed directly in (ψ, θ, α) field-line-following coordinates, the red lines are results computed in cylindrical coordinates and then interpolated to the field-line-following coordinates. There is systematical discrepancy between ψ computed by the two methods. The results are actually very close to each other and the difference becomes obvious because the variation of ψ is very small for a passing electron.

The results of α from the two methods also agree with each other. The discrepancy near $t\Omega_i = 400$ is due to that α is close to 2π, and one result becomes zero, which is equivalent to 2π.

equilibrium is the DIID-D cyclone base case

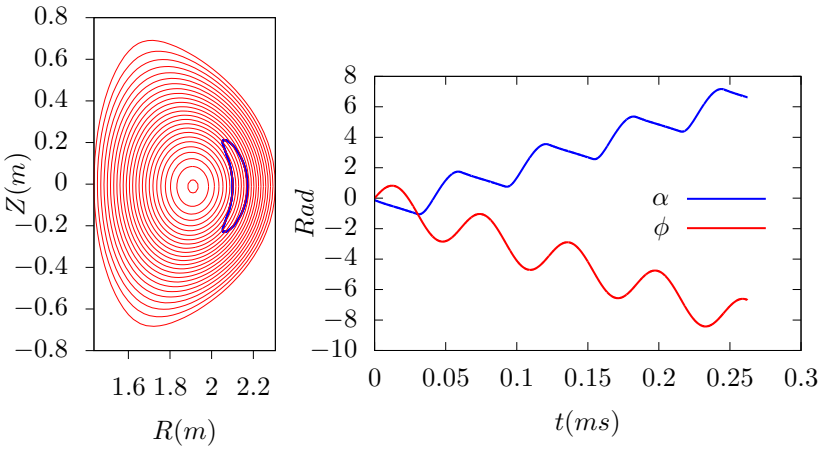

Figure 4. Left: orbit on poloidal plane. Right: α is defined by $\alpha = \phi - \int_0^\theta \hat{q} d\,\theta$, where ϕ is the usual cylindrical toroidal angle.

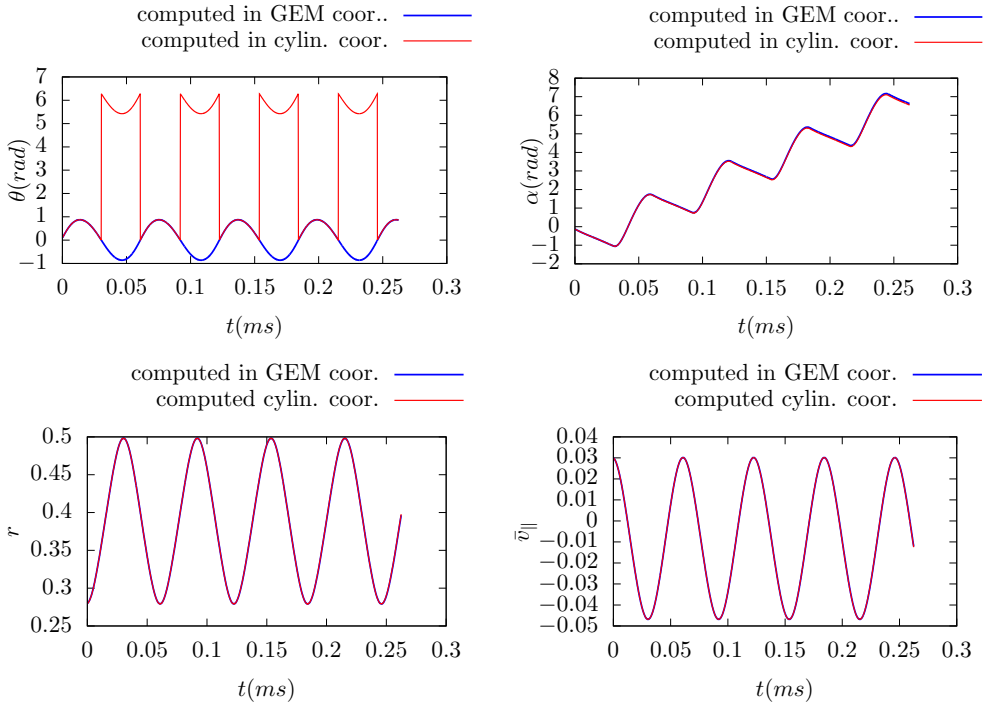

Figure 5. The evolutions of the poloidal angles θ and generalized toroidal angle α calculated by the two methods agree with each other. $r=\sqrt{\frac{\Psi-\Psi_0}{\Psi_b-\Psi_0}}$

3 Equations of motion in cylindrical coordinates

In this section, all quantities are in the normalized form given in Sec. 1.1. For notational simplicity, the over-bars of the notation are omitted. In cylindrical coordinates $(R,\,\phi,\,Z)$, the location vector is written as $\mathbf{X}=R\hat{\mathbf{e}}_R(\phi)+Z\hat{\mathbf{e}}_Z$. Using this, we obtain

$$\begin{aligned}\frac{d\mathbf{X}}{dt} &= \frac{dR}{dt}\hat{\mathbf{e}}_R+R\frac{d\hat{\mathbf{e}}_R(\phi)}{dt}+\frac{dZ}{dt}\hat{\mathbf{e}}_Z\\ &= \frac{dR}{dt}\hat{\mathbf{e}}_R+R\frac{d\phi}{dt}\hat{\mathbf{e}}_\phi+\frac{dZ}{dt}\hat{\mathbf{e}}_Z.\end{aligned}\tag{39}$$

Substituting this into Eq. (1) gives

$$\frac{dR}{dt}\hat{\mathbf{e}}_R+R\frac{d\phi}{dt}\hat{\mathbf{e}}_\phi+\frac{dZ}{dt}\hat{\mathbf{e}}_Z=\frac{\mathbf{B}^\star}{B^\star_{\|}}v_{\|}+\frac{\mu}{2\pi BB^\star}\mathbf{B}\times\nabla B+\frac{1}{BB^\star_{\|}}\mathbf{E}\times\mathbf{B},\tag{40}$$

from which we obtain the following component equations:

$$\frac{dR}{dt}=\left[\frac{\mathbf{B}^\star}{B^\star_{\|}}v_{\|}+\frac{\mu}{2\pi BB^\star_{\|}}\mathbf{B}\times\nabla B+\frac{1}{BB^\star_{\|}}\mathbf{E}\times\mathbf{B}\right]\cdot\hat{\mathbf{e}}_R\tag{41}$$

$$\frac{dZ}{dt}=\left[\frac{\mathbf{B}^\star}{B^\star_{\|}}v_{\|}+\frac{\mu}{2\pi BB^\star_{\|}}\mathbf{B}\times\nabla B+\frac{1}{BB^\star_{\|}}\mathbf{E}\times\mathbf{B}\right]\cdot\hat{\mathbf{e}}_Z,\tag{42}$$

$$\frac{d\phi}{dt}=\frac{1}{R}\left[\frac{\mathbf{B}^\star}{B^\star_{\|}}v_{\|}+\frac{\mu}{2\pi BB^\star_{\|}}\mathbf{B}\times\nabla B+\frac{1}{BB^\star_{\|}}\mathbf{E}\times\mathbf{B}\right]\cdot\hat{\mathbf{e}}_\phi,\tag{43}$$

In the cylindrical coordinates, the terms $\mathbf{B}\times\nabla B$, $\nabla\times\mathbf{b}$, and $\mathbf{b}\cdot\nabla\times\mathbf{b}$ are written, respectively, as

$$\mathbf{B}\times\nabla B = \begin{vmatrix} \hat{e}_R & \hat{e}_\phi & \hat{e}_Z \\ B_R & B_\phi & B_Z \\ \frac{\partial B}{\partial R} & \frac{1}{R}\frac{\partial B}{\partial \phi} & \frac{\partial B}{\partial Z} \end{vmatrix}, \tag{44}$$

$$\nabla\times\mathbf{b} = \left(\frac{1}{R}\frac{\partial b_Z}{\partial\phi}-\frac{\partial b_\phi}{\partial z}\right)\hat{e}_R+\left(\frac{\partial b_R}{\partial Z}-\frac{\partial b_Z}{\partial R}\right)\hat{e}_\phi+\left(\frac{1}{R}\frac{\partial(Rb_\phi)}{\partial R}-\frac{1}{R}\frac{\partial b_R}{\partial\phi}\right)\hat{e}_Z, \tag{45}$$

$$\mathbf{b}\cdot\nabla\times\mathbf{b} = b_R\left(\frac{1}{R}\frac{\partial b_Z}{\partial\phi}-\frac{\partial b_\phi}{\partial z}\right)+b_\phi\left(\frac{\partial b_R}{\partial Z}-\frac{\partial b_Z}{\partial R}\right)+b_Z\left(\frac{1}{R}\frac{\partial(Rb_\phi)}{\partial R}-\frac{1}{R}\frac{\partial b_R}{\partial\phi}\right). \tag{46}$$

Using $b_R=\frac{B_R}{B}$, $b_Z=\frac{B_Z}{B}$, and $b_\phi=\frac{B_\phi}{B}$, we obtain

$$\begin{cases} \frac{\partial b_R}{\partial R}=\frac{\frac{\partial B_R}{\partial R}B-\frac{\partial B}{\partial R}B_R}{B^2} \\ \frac{\partial b_R}{\partial Z}=\frac{\frac{\partial B_R}{\partial Z}B-\frac{\partial B}{\partial Z}B_R}{B^2} \\ \frac{\partial b_R}{\partial\phi}=\frac{\frac{\partial B_R}{\partial\phi}B-\frac{\partial B}{\partial\phi}B_R}{B^2} \end{cases} \quad \begin{cases} \frac{\partial b_Z}{\partial R}=\frac{\frac{\partial B_Z}{\partial R}B-\frac{\partial B}{\partial R}B_Z}{B^2} \\ \frac{\partial b_Z}{\partial Z}=\frac{\frac{\partial B_Z}{\partial Z}B-\frac{\partial B}{\partial Z}B_Z}{B^2} \\ \frac{\partial b_Z}{\partial\phi}=\frac{\frac{\partial B_Z}{\partial\phi}B-\frac{\partial B}{\partial\phi}B_Z}{B^2} \end{cases} \quad \begin{cases} \frac{\partial b_\phi}{\partial R}=\frac{\frac{\partial B_\phi}{\partial R}B-\frac{\partial B}{\partial R}B_\phi}{B^2} \\ \frac{\partial b_\phi}{\partial Z}=\frac{\frac{\partial B_\phi}{\partial Z}B-\frac{\partial B}{\partial Z}B_\phi}{B^2} \\ \frac{\partial b_\phi}{\partial\phi}=\frac{\frac{\partial B_\phi}{\partial\phi}B-\frac{\partial B}{\partial\phi}B_\phi}{B^2} \end{cases} \tag{47}$$

The equation for $v_\parallel$ is given by Eq. (11), i.e.,

$$\frac{dv_\parallel}{dt}=-\mu\frac{\mathbf{B}^\star}{B_\parallel^\star}\cdot\nabla B+2\pi\frac{\mathbf{B}^\star}{B_\parallel^\star}\cdot\mathbf{E}. \tag{48}$$

The first term on the left-hand-side is written

$$\frac{\mathbf{B}^\star}{B_\parallel^\star}\cdot\nabla B=\frac{B_R^\star}{B_\parallel^\star}\frac{\partial B}{\partial R}+\frac{B_\phi^\star}{B_\parallel^\star}\frac{1}{R}\frac{\partial B}{\partial\phi}+\frac{B_Z^\star}{B_\parallel^\star}\frac{\partial B}{\partial Z}, \tag{49}$$

where

$$B_R^\star=B_R+\frac{v_\parallel}{2\pi}\left(\frac{1}{R}\frac{\partial b_Z}{\partial\phi}-\frac{\partial b_\phi}{\partial z}\right), \tag{50}$$

$$B_Z^\star=B_Z+\frac{v_\parallel}{2\pi}\left(\frac{1}{R}\frac{\partial(Rb_\phi)}{\partial R}-\frac{1}{R}\frac{\partial b_R}{\partial\phi}\right), \tag{51}$$

$$B_\phi^\star=B_\phi+\frac{v_\parallel}{2\pi}\left(\frac{\partial b_R}{\partial Z}-\frac{\partial b_Z}{\partial R}\right), \tag{52}$$

and $B_\parallel^\star$ is given by Eq. (13).

4 Code Benchmarking

4.1 Initial conditions

The initial conditions of the particle are given by specifying the initial location (R,ϕ,Z), initial parallel velocity $v_\parallel$, and the magnetic moment μ (which acts as a parameter since μ is exactly conserved). In some cases, we prefer to specify the initial velocity in terms of the initial kinetic energy ε and the initial pitch angle θ (the include angle between velocity and the local magnetic field). The relation between (ε,θ) and $(v_\parallel,\mu)$ is given by

$$\mu=\frac{mv_\perp^2}{2B}=\frac{mv^2}{2B}\sin^2\theta=\frac{\varepsilon}{B}\sin^2\theta, \tag{53}$$

and

$$v_{\|} = v\sin\theta = \sqrt{\frac{2\varepsilon}{m}}\cos\theta. \tag{54}$$

The relation between (ε, θ) and the normalized quantities $(\bar{\mu}, \bar{v}_{\|})$ is given by

$$\bar{\mu} = \frac{\mu}{\mu_n} = \frac{\varepsilon}{B}\sin^2\theta\,\frac{1}{mv_n^2/B_n} = \frac{\varepsilon}{mv_n^2\bar{B}}\sin^2\theta, \tag{55}$$

and

$$\bar{v}_{\|} = \sqrt{\frac{2\varepsilon}{mv_n^2}}\cos\theta. \tag{56}$$

4.2 Constants of motion

There are three constants of motion for the guiding center motion, namely, the canonical toroidal angular momentum P_ϕ, the magnetic moment μ, and the total kinetic energy ε. Examining how well the kinetic energy ε and the toroidal angular momentum P_ϕ are conserved provides a way to evaluate the accuracy of the numerical code. The kinetic energy ε and toroidal angular momentum P_ϕ are defined by

$$\varepsilon = \frac{1}{2}mv^2 = \frac{1}{2}mv_{\|}^2 + B\mu \tag{57}$$

$$P_\phi = m\frac{g(\Psi)}{B}v_{\|} + Ze\Psi, \tag{58}$$

Define $\varepsilon_n = mv_n^2$ and $P_{\phi n} = ZeB_nL_n^2$, then the normalized forms of ε and P_ϕ are written as

$$\bar{\varepsilon} \equiv \frac{\varepsilon}{mv_n^2} = \frac{1}{2}\bar{v}_{\|}^2 + \bar{\mu}\bar{B} \tag{59}$$

$$\begin{aligned}\bar{P}_\phi &\equiv \frac{P_\phi}{P_{\phi n}} \\ &= \frac{1}{2\pi}\,\bar{g}\,\frac{\bar{v}_{\|}}{\bar{B}} + \bar{\Psi}\end{aligned} \tag{60}$$

Figure 6 plots the time evolution of the kinetic energy $\bar{\varepsilon}$ and toroidal angular momentum $\bar{P}_\phi$ for an energetic ion in EAST magnetic configuration. The results shows that $\bar{\varepsilon}$ and $\bar{P}_\phi$ are conserved to acceptable accuracy for 100 poloidal periods of the orbit.

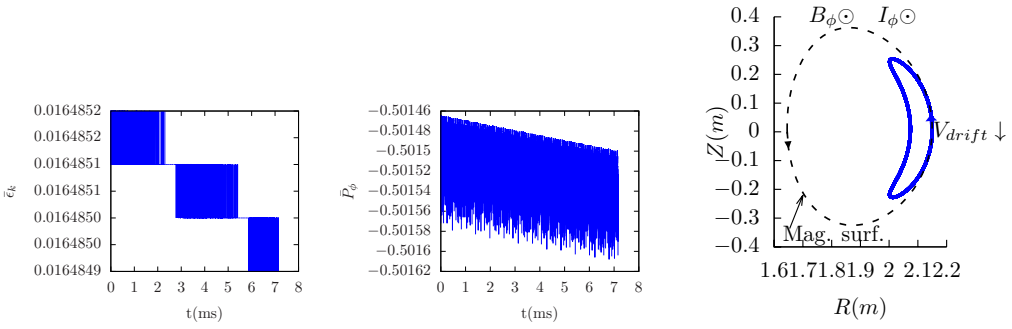

Figure 6. Time evolution of the kinetic energy $\bar{\varepsilon}$ (a) and toroidal angular momentum $\bar{P}_\phi$ (b) for a Deuteron of 20keV launched at the low-field-side midplane ($R_{\rm ini} = 2.15m$, $Z_{\rm ini} = 0m$) with pitch angle $\theta = 75°$. The results shows that $\bar{\varepsilon}$ and $\bar{P}_\phi$ are conserved to acceptable accuracy ($\bar{\varepsilon}_k$ decreased by 1.8×10^{-5} and $\bar{P}_\phi$ by 3.2×10^{-4} during the time of 100 poloidal periods). The corresponding poloidal orbit is plotted in (c). Fourth-order Runge-Kutta time advancing scheme is used in integrating the orbit with a time step of 1 / 183 poloidal period. The magnetic equilibrium is from EAST discharge #62585@2.8s (gfile provided by ZhengZheng).

5 Orbit classification

A particle whose $v_\parallel$ takes the same sign during one poloidal period is called a passing particle. Otherwise, it is called a trapped particle.

For a particle with a given initial condition, can we determine whether the particle is passing or not, without numerically computing its orbit (and without assuming zero orbit width)? The answer is yes. We can do this by making use of the conservation of P_ϕ, μ, and the kinetic energy ε.

$$P_\phi = m\frac{g}{B}v_\parallel + Ze\Psi, \tag{61}$$

$$\mu = \frac{m}{2B}v_\perp^2, \tag{62}$$

$$\varepsilon = \frac{1}{2}m\,(v_\perp^2 + v_\parallel^2), \tag{63}$$

The critical condition for a particle being passing/trapped is that its parallel velocity $v_\parallel$ is zero on the high-field side of the midplane. (For a given magnetic surface, the midplane can be defined as the poloidal locations where $\partial B\,/\,\partial\theta = 0$. For simple magnetic magnetic surfaces, usually there are two poloidal locations satisfying $\partial B\,/\,\partial\theta = 0$ and we denote these two locations by $\theta = -\pi$ (high-field-side) and $\theta = 0$ (low-field-side), respectively.)

Define a dimensionless variable Λ by

$$\Lambda = \frac{\mu B_{\text{axis}}}{\varepsilon}, \tag{64}$$

which is a constant of motion, and is often used as a phase space coordinate in place of μ. What does the above critical condition look like in (P_ϕ, Λ) space? Using $v_\parallel = 0$, Eq. (61) is reduced to

$$P_\phi = Ze\Psi, \tag{65}$$

which determines Ψ if P_ϕ is given. Using $v_\parallel = 0$, expression (64) is written as

$$\Lambda = \frac{B_{\text{axis}}}{B}. \tag{66}$$

Since the critical condition requires $\theta = -\pi$. Therefore Eq. (66) is written as

$$\Lambda = \frac{B_{\text{axis}}}{B(\theta = -\pi)}, \tag{67}$$

The curve in the (P_ϕ, Λ) plane corresponding to the critical condition can be traced out in the following steps: 1. for a given P_ϕ, use Eq. (65) to determine Ψ and hence a magnetic surface; 2. the value of $B(\theta = -\pi)$ on the magnetic surface can be determined; 3. then the value of Λ can be determined by Eq. (67).

The curve traced out by the above method for an EAST magnetic configuration is plotted in Fig. 7, where the black curve corresponds to Eq. (67). The region above the black line is the trapped region, and that below it is the passing region.

Another curve similar to Eq. (67) is

$$\Lambda = \frac{B_{\text{axis}}}{B(\theta = 0)}, \tag{68}$$

This is plotted as blue curve in Fig. 7. This curve is approximately the phase space boundary beyond which no physical particles exist. (There is actually a small region where physical particles can exit beyond the blue curve, which corresponds to the stagnation orbits. This region is usually very small, see Fig. 10).

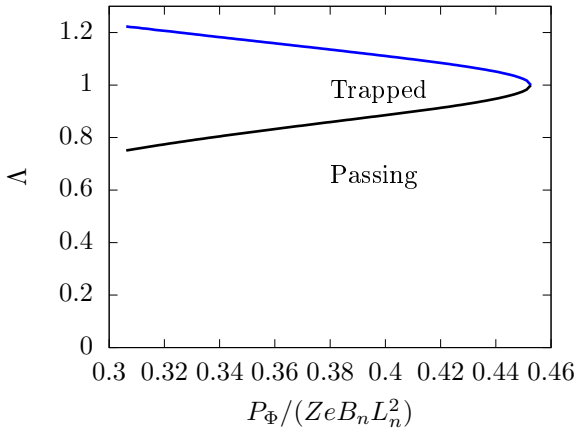

Figure 7. The region between the lower part (black line) and the upper part (blue line) of the curve is the trapped region. The region below the lower part of the curve is the passing region.

Note that, in determine the passing trapped boundary in the (P_ϕ, Λ) plane, we do not need to specify the kinetic energy ε. The reason for this is as follows. Using Eqs. (62) and (63) to eliminate $v_\parallel$ in Eq. (61), we obtain an equation in the (P_ϕ, Λ) plane:

$$2(\varepsilon - B\mu) - \frac{1}{m}(P_\phi - Ze\Psi)^2\left(\frac{B}{g}\right)^2 = 0, \tag{69}$$

i.e.,

$$\Lambda = -\frac{BB_{\text{axis}}}{g^2}\frac{1}{2m\varepsilon}(P_\phi - Ze\Psi)^2 + \frac{B_{\text{axis}}}{B}, \tag{70}$$

where the dependence on ε disappears because the critical condition requires that $P_\phi - Ze\Psi = 0$.

Next, let us consider the phase space points with a given kinetic energy and a given spatial location, and examine how these points are distributed in the (P_ϕ, Λ) plane. Note that Eq. (70) involve two free parameters Ψ and B. Let us first fixed the value of Ψ. Then there remains a free parameter B to be chosen. Two representative values of B are $B(\theta = -\pi)$ and $B(\theta = 0)$, corresponding to, respectively, the maximum and minimum of B on the the given magnetic surface. If the given magnetic surface corresponds to the magnetic axis, then $B(\theta = -\pi)$ and $B(\theta = 0)$ are identical. Figure 8 plots the three curves that correspond to the LCFS with $\theta = -\pi$, the LCFS with $\theta = 0$, and the magnetic axis, respectively.

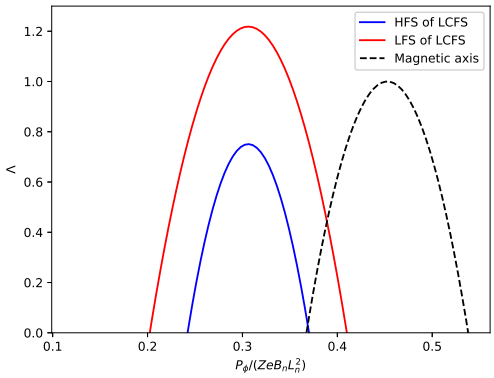

Figure 8. The magnetic axis (black dash), high-field-side (blue) and low-field side (red) of LCFS mapped to the (P_ϕ, Λ) plane. For $E = 50$keV, EAST#52340

Next, let us consider all the physically possible points in the phase space (P_ϕ, Λ) for a given kinetic energy and a given spatial region. Note that Eq. (70) involves two free parameters Ψ and B, both of which are functions of spatial locations. For each value of P_ϕ, scan the spatial region to find all the values of Λ by using Eq. (70). Denote the range of Λ for a specific value of P_ϕ by $[\Lambda_{\min}: \Lambda_{\max}]$. If $\Lambda_{\max} < 0$, then this indicates this value of P_ϕ is not physically possible. If $\Lambda_{\max} \geqslant 0$, then this value of P_ϕ is physically possible and the physically possible range of Λ for this value of P_ϕ is $[0: \Lambda_{\max}]$. Figure 9 plots the curve $\Lambda = \Lambda_{\max}(P_\phi)$ for $\Lambda_{\max} \geqslant 0$.

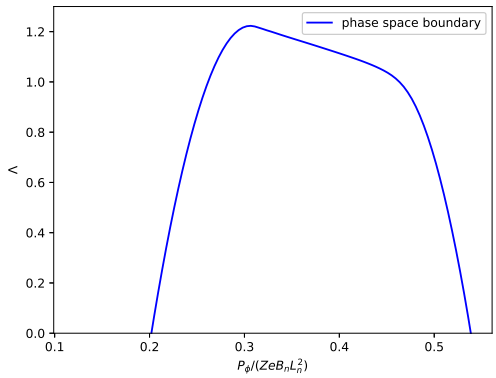

Figure 9. Boundary of phase space (P_ϕ, Λ). For $E = 50$keV, EAST#52340

Putting results in Fig. 7, 8, and 9 into one figure, we obtain Fig. 10.

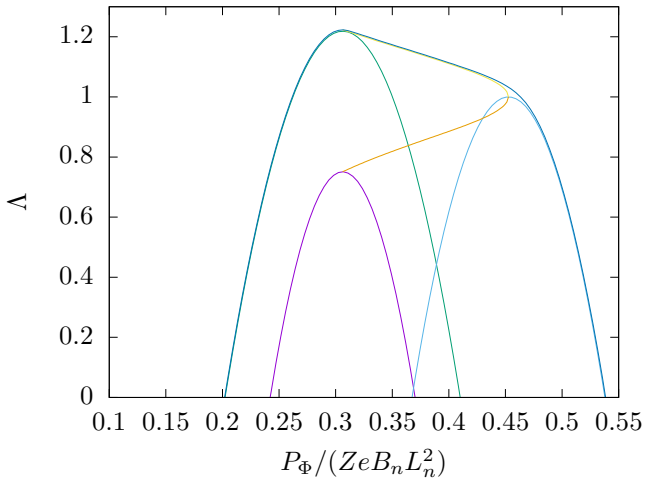

Figure 10. Results in Fig. 7, 8, and 9 plotted in one figure. For $E = 50$keV, EAST#52340.

5.1 Numerically testing orbit types

In the above, we plot boundary curves in the phase space (P_ϕ, Λ) and get some rough ideas about possible orbits in different regions of (P_ϕ, Λ) plane. Next, let us numerically examine the orbits and confirm which regions are corresponding to passing/trapped/confined/lost regions.

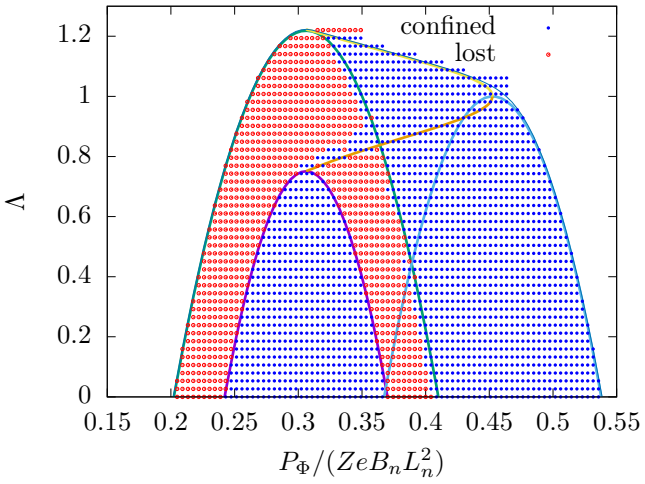

Figure 11. For $E = 50$keV, EAST#52340. Orbits are numerically computed to check whether they are confined (not touch the LCFS) or lost (touch the LCFS). Some particles in the loss region are numerically determined to be confined. Whether this is due to numerical errors is unclear.

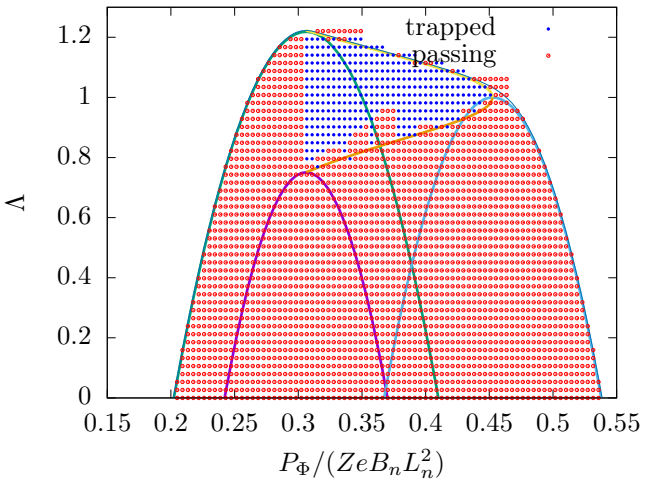

Figure 12. For $E = 50$keV, EAST#52340. Orbits are numerically computed to check whether they are passing or trapped. Some particles in the trapped region are numerically determined to be passing. Whether this is due to numerical errors is unclear.

$$\bar{P}_\phi = \frac{P_\phi}{ZeB_nL_n^2} \tag{71}$$

$$-\frac{BB_{\text{axis}}}{g^2}\frac{1}{2m\varepsilon}(P_\phi - Ze\Psi)^2$$

$$\begin{aligned}
&-\frac{BB_{\text{axis}}}{g^2}\frac{1}{2m\varepsilon}(P_\phi - Ze\Psi)^2 \\
=&-\frac{\overline{B}\,\overline{B}_{\text{axis}}}{\bar{g}^2}\frac{m}{2m^2\varepsilon}L_n^2(ZeB_n)^2(\bar{P}_\phi - \overline{\Psi})^2 \\
=&-\frac{\overline{B}\,\overline{B}_{\text{axis}}}{\bar{g}^2}\frac{m}{2\varepsilon}L_n^2\Omega_n^2(\bar{P}_\phi - \overline{\Psi})^2 \\
=&-\frac{\overline{B}\,\overline{B}_{\text{axis}}}{\bar{g}^2}\frac{m}{2\varepsilon}L_n^2\frac{(2\pi)^2}{T_n^2}(\bar{P}_\phi - \overline{\Psi})^2 \\
=&-\frac{\overline{B}\,\overline{B}_{\text{axis}}}{\bar{g}^2}\frac{m}{2\varepsilon}v_n^2(2\pi)^2(\bar{P}_\phi - \overline{\Psi})^2
\end{aligned}$$

$$=-\frac{\overline{B}\,\overline{B}_{\rm axis}}{\bar{g}^2}\frac{1}{2\bar{\varepsilon}}(2\pi)^2(\bar{P}_\phi-\overline{\Psi})^2$$

$$m\frac{g}{B}v_\parallel = P_\phi - Ze\Psi, \tag{72}$$

$$\bar{v}_\parallel = \frac{v_\parallel}{v_n} = \frac{BZeB_nL_n^2}{mg\frac{L_n}{T_n}}(\bar{P}_\phi-\overline{\Psi}). \tag{73}$$

$$\bar{v}_\parallel = \frac{\overline{B}\Omega_n T_n}{\bar{g}}(\bar{P}_\phi-\overline{\Psi}) \tag{74}$$

$$\bar{v}_\parallel = \frac{\overline{B}\frac{|Z|}{Z}2\pi}{\bar{g}}(\bar{P}_\phi-\overline{\Psi}) \tag{75}$$

5.2 Trapped passing boundary in the zero-orbit-width limit

An approximate condition determining whether a particle is trapped or circulating can be obtained by using the conservation of magnetic moment and kinetic energy, and assuming the guiding center orbit is along the magnetic field line (zero-width orbit approximation, which is a proper approximation for low-energy particles whose orbit width is small, as is shown in Fig. 13).

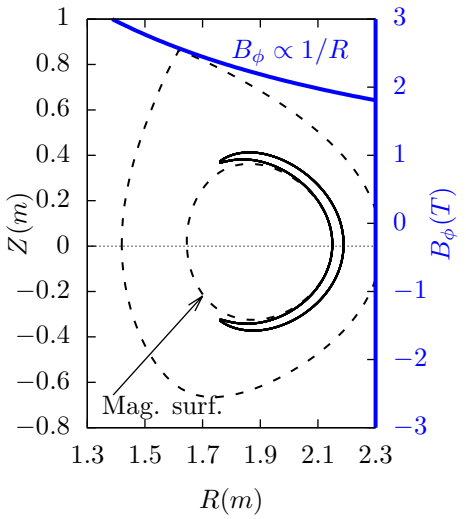

Figure 13. The magnetic field becomes stronger when a particle move inboard (toward smaller R). Due to the conservation of kinetic energy and magnetic moment, the magnitude of the parallel velocity decrease when a particle moves inboard. Also shown is the poloidal projection of guiding-center orbit for a particle of energy 2keV launched in the low-field-side midplane ($R=2.25m$, $Z=0m$) with a pitch angle $\theta=115°$.

In this approximation, the orbit remains on a magnetic surface. The critical condition for a particle to be trapped/circulating is given by

$$\frac{mv_\perp^2}{2B} = \frac{mv^2}{2B_{\rm max}}, \tag{76}$$

where $v_\perp$ is the perpendicular (to the magnetic field) velocity of the particle at the location where the strength of the magnetic field is B, $B_{\max}$ is the maximum value of the magnetic field on the same magnetic surface where the particle moves. Define $\theta = \arccos(v_\parallel / v)$, which is the pitch angle of velocity with respect to the local magnetic field, then Eq. (76) is written as

$$\cos^2\theta = 1 - \frac{B}{B_{\max}}. \tag{77}$$

Define

$$\theta_c = \arccos\left(\sqrt{1 - \frac{B}{B_{\max}}}\right), \tag{78}$$

then particles with $\theta_c < \theta < \pi - \theta_c$ can not reach the point of the maximum magnetic field of the same magnetic surface and thus they are trapped particles. Otherwise, they are circulating particles. In velocity space $(v_\parallel, v_\perp)$, the trapped and circulating region are shown in Fig. 14.

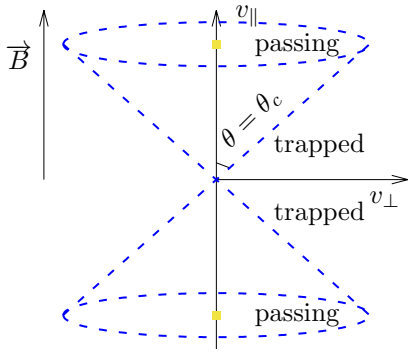

Figure 14. Passing and trapped regions in the phase-space $(v_\parallel, v_\perp)$. The trapped region is $\theta_c < \theta < \pi - \theta_c$.

Note that the trapped-circulating boundary given in Fig. 14 is determined based on the assumption that the guiding center motion does not deviate from a magnetic surface. However, the actual guiding center orbit does not remain on the same magnetic surface, so the above result can be wrong when applied to some particles. An example is given in Fig. 15, where the numerical results show that the particle is actually trapped but the approximate condition indicate that the particle is circulating.

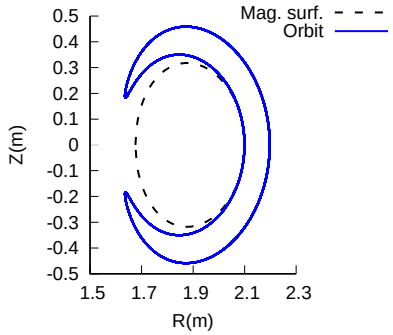

Figure 15. Numerical orbit of a particle on the poloidal plane, which show that the particle is trapped. However, the particle would be considered to be circulating if we used the approximate condition given in Fig. 14. It is easy to understand why the approximate condition breaks down for this case: the orbit deviates from the original flux surface (i.e., the zero-width orbit) to the stronger field region.

At a given radial location, in terms of (w, μ) coordinates, where w is the kinetic energy, the trapped passing boundary is shown in Fig. 16.

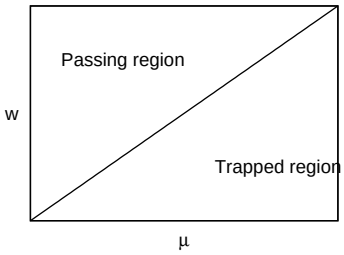

Figure 16. The passing and trapped regions of phase space (w, μ). The boundary between passing and trapped region is given by $w = \mu B_{\max}$, where $B_{\max}$ is the maximum value of magnetic field on the same magnetic surface where the particle moves (zero orbit width is assumed).

5.3 Trapped particle fraction

The trapped particle fraction f_t is defined as the ratio of the number of trapped particles to the total number of particles. Particle distribution function (in terms of guiding-center variables) can be written as $f = f(\mathbf{r}, v, \theta, \phi)$, where $\mathbf{r}$ is the guiding-center position vector in configuration space and (v, θ, ϕ) is the spherical coordinates in velocity space with θ being the pitch angle and ϕ the gyro-angle. Assuming zero Larmor radius limit, then the trapped particle fraction f_t is written as

$$f_t(\mathbf{r}) = \frac{\int_0^{\infty}\int_{\theta_c}^{\pi-\theta_c}\int_0^{2\pi} f(\mathbf{r}, v, \theta, \phi) v^2 \sin\theta dv d\theta d\phi}{\int_0^{\infty}\int_0^{\pi}\int_0^{2\pi} f(\mathbf{r}, v, \theta, \phi) v^2 \sin\theta dv d\theta d\phi}, \tag{79}$$

where θ_c is the critical pitch angle defined in Sec. 5. Assume that $f(\mathbf{r}, v, \theta, \phi)$ is uniform in θ and ϕ, then the integration over the θ and ϕ in Eq. (79) can be performed, giving

$$\begin{aligned} f_t(\mathbf{r}) &= \frac{2\pi \times 2\cos\theta_c \int_0^{\infty} f(\mathbf{r}, v) v^2 dv}{4\pi \int_0^{\infty} f(\mathbf{r}, v) v^2 dv} \\ &= \cos\theta_c. \end{aligned} \tag{80}$$

Using the definition of the critical value of the pitch angle (Eq. (78)), the above expression is written as

$$f_t(\mathbf{r}) = \sqrt{1 - \frac{B}{B_{\max}}}. \tag{81}$$

The flux surface averaging of f_t, $\langle f_t \rangle$, is written as

$$\begin{aligned} \langle f_t \rangle &= \left\langle \sqrt{1 - \frac{B}{B_{\max}}} \right\rangle \\ &= \frac{\oint \sqrt{1 - \frac{B}{B_{\max}}} \frac{1}{B_p} dl_p}{\oint \frac{1}{B_p} dl_p} \end{aligned}$$

How to relate $\langle f_t \rangle$ to the following neoclassical effective trapped fraction?

$$f_{t,\mathrm{neo}} = 1 - \frac{3}{4}\left\langle \frac{B^2}{B_{\max}^2} \right\rangle \int_0^1 \frac{\lambda d\lambda}{\left\langle \sqrt{1 - \lambda B / B_{\max}} \right\rangle}. \tag{82}$$

5.3.1 For circular flux surface with large aspect ratio

In the large aspect ratio approximation and for particles that are initially on the low-field-side of the midplane, Eq. (81) is written

$$f_t = \sqrt{1 - \frac{R_0 - r}{R_0 + r}} = \sqrt{\frac{2r}{R_0 + r}} \approx \sqrt{2\varepsilon}, \tag{83}$$

where $\varepsilon = r/R_0$. This is the result given in Wessson's book[2]. Note that this result is valid only for particles that are initially at the low-field-side of the midplane. For particles that are initially located at the poloidal location θ_p, the trapped particles fraction is written

$$f_t = \sqrt{1 - \frac{R_0 - r}{R_0 + r\cos\theta_p}} = \sqrt{\frac{r(1+\cos\theta_p)}{R_0 + r\cos\theta_p}}, \tag{84}$$

For $\theta_p = \pi$, i.e., at the high-field-side of the midplane, $f_t = 0$, i.e., there is no trapped particles there.

Using Eq. (84), the flux surface averaging of f_t, $\langle f_t \rangle$, is written as

$$\begin{aligned}
\langle f_t \rangle &= \frac{\oint f_t \frac{1}{B_p} dl_p}{\oint \frac{1}{B_p} dl_p} \\
&= \frac{\oint \sqrt{\frac{r(1+\cos\theta_p)}{R_0 + r\cos\theta_p}} \frac{1}{B_p} dl_p}{\oint \frac{1}{B_p} dl_p} \\
&= \frac{\oint \sqrt{\frac{r(1+\cos\theta_p)}{R_0 + r\cos\theta_p}} \frac{1}{B_p} r\, d\theta}{\oint \frac{1}{B_p} r\, d\theta}
\end{aligned}$$

5.4 Bounce frequency of deeply trapped particles

Let us analytically estimate the bounce frequency of deeply trapped particles. The time evolution of the parallel velocity of a guiding center is given by Eq. (2), i.e.,

$$\frac{dv_\parallel}{dt} = -\frac{\mu}{m} \frac{\mathbf{B}^\star}{B^\star_\parallel} \cdot \nabla B, \tag{85}$$

which can be approximately written as

$$\frac{dv_\parallel}{dt} = -\frac{\mu}{m} \mathbf{b} \cdot \nabla B,$$

which can be further written as

$$\frac{d^2 l}{dt^2} = -\frac{v_\perp^2}{2B} \frac{dB}{dl} \tag{86}$$

where dl is the arc length along the magnetic field. In a large aspect ratio tokamak with circular flux surfaces, the magnetic field can be written approximately as

$$B = \frac{B_0}{1 + (r/R_0)\cos\theta}, \tag{87}$$

The equation of magnetic field is written

$$\frac{B_\theta}{B} = \frac{dl_p}{dl} = \frac{r\, d\theta}{dl}, \tag{88}$$

which can be written

$$dl = \frac{B}{B_\theta} r\, d\theta \tag{89}$$

Using Eqs. (89) and (87), the parallel derivative of the magnetic field is written as

$$\frac{dB}{dl} = \frac{B_\theta}{rB} \frac{dB}{d\theta} = \frac{B_\theta}{rB} \frac{B_0}{[1 + (r/R_0)\cos\theta]^2} \frac{r}{R_0} \sin\theta, \tag{90}$$

Plug this into equation (86), then we obtain

$$\frac{d^2l}{dt^2} = -\frac{v_\perp^2}{2B}\frac{B_\theta}{rB}\frac{B_0}{[1+(r/R_0)\cos\theta]^2}\frac{r}{R_0}\sin\theta = -\frac{v_\perp^2}{2}\frac{B_\theta}{B_0}\frac{1}{R_0}\sin\theta \tag{91}$$

Consider deeply trapped particles (particles are trapped in a very small region near the low-field-side midplane), i.e., $\theta \approx 0$, then we have $\sin\theta \approx \theta$. Using this, the above equation is written as

$$\frac{d^2l}{dt^2} \approx -\frac{v_\perp^2}{2}\frac{B_\theta}{B_0}\frac{1}{R_0}\theta \tag{92}$$

Assume the orbit is along the magnetic field line (i.e. zero-width orbit approximation), then the equation of magnetic field (89) is also satisfied by the orbit. In the linear approximation, we have $\theta \approx B_\theta/(Br)l$. Using this in Eq. (92), we obtain

$$\frac{d^2l}{dt^2} = -\frac{rv_\perp^2}{2R_0}\frac{B_\theta^2}{B^2r^2}l \tag{93}$$

Using the definition of safety factor, $q = rB_0/R_0B_\theta$, the above equation is written

$$\frac{d^2l}{dt^2} = -\frac{v_\perp^2}{q^2R_0^2}\frac{r}{2R_0}l \tag{94}$$

Define

$$\omega_b = \frac{v_\perp}{qR_0}\left(\frac{r}{2R_0}\right)^{1/2}, \tag{95}$$

(for deeply trapped particles, the variation of $v_\perp$ during one poloidal period is small, and thus can be considered constant, and thus ω_b can also be considered constant), then Eq. (94) is written

$$\frac{d^2l}{dt^2} = -\omega_b^2 l, \tag{96}$$

which indicates that the motion of a deeply trapped particle is a harmonic oscillation with an angular frequency ω_b. Equations (95) and (96) agree with Eqs. (3.12.3) and (3.12.4) in Wesson's book "Tokmaks"[2]. I have test the accuracy of formula (95) by comparing it with the numerical results, which indicates the formula can usually give a reasonable estimation of the bounce frequency (for example, 28kHz is obtained numerically while the analytical formula gives 24kHz for a not very deeply trapped orbit).

5.5 Bounce frequency of barely trapped particles

Let us analytically estimate the bounce frequency of barely trapped particles, i.e., particle satisfying the critical condition (76),

$$\left(\frac{v_\parallel}{v}\right)^2 = 1 - \frac{B}{B_{\max}} \approx 1 - \frac{R_0 - r}{R_0 + r} \approx 2\varepsilon, \tag{97}$$

i.e., $v_\parallel = \sqrt{2\varepsilon}v$, where $v_\parallel$ is the parallel velocity on the low-field-side midplane.

The distance along the magnetic field line traveled in half an orbit is about $2\pi R_0 q$, then the time needed is then given by

$$t_b \approx \frac{2\pi R_0 q}{v_\parallel} \approx \frac{2\pi R_0 q}{\sqrt{2\varepsilon}v} \approx \frac{2\pi R_0 q}{\sqrt{2\varepsilon}v_{\text{th}}} \tag{98}$$

The above approximation is rough since $v_\parallel$ changes between zero and $\sqrt{2\varepsilon}v$ and we still use a constant value, $\sqrt{2\varepsilon}v$, in approximating it.

Then the bounce (angular) frequency is given by

$$\omega_b = \frac{2\pi}{2t_b} = \frac{2\pi}{4\pi R_0 q}\sqrt{2\varepsilon}v_{\text{th}} = \frac{v_{\text{th}}}{R_0 q}\sqrt{\frac{\varepsilon}{2}}, \tag{99}$$

which turns out to be take the same form as Eq. (95). very strange!

5.6 Methods of determining drift orbits

If neglecting the magnetic drift, a guiding-center orbit is along a magnetic field lines, i.e., there is no derivation from the magnetic surface where a guiding center is initially located. Taking the magnetic drift into account, a guiding-center orbit will deviate from the initial magnetic surface, giving an orbit of nonzero width in the poloidal plane.

Whether a guiding-center will drift radially outward or inward from a local magnetic surface near the midplane can be determined in the following way. First note that the zero-order approximation of the guiding-center orbit (zero-width orbit) is either parallel or anti-parallel to the local magnetic field, depending on the sign of $v_\parallel$. Further note the direction of the magnetic drift ($\frac{Z}{|Z|}\mathbf{B}\times\nabla B$ and curvature drift) is approximately vertical, which can be either up or down, depending on the charge sign and direction of the toroidal magnetic field. Finally, by imposing the magnetic drift on the zero-width orbit, we can determine whether the guiding center will drift inward or outward from the local magnetic surface. Figures 17-19 plots the drift orbits for all the possible combinations of tokamak magnetic configurations and particle initial conditions (assume particles of positive charge, i.e., $Z/|Z|>0$).

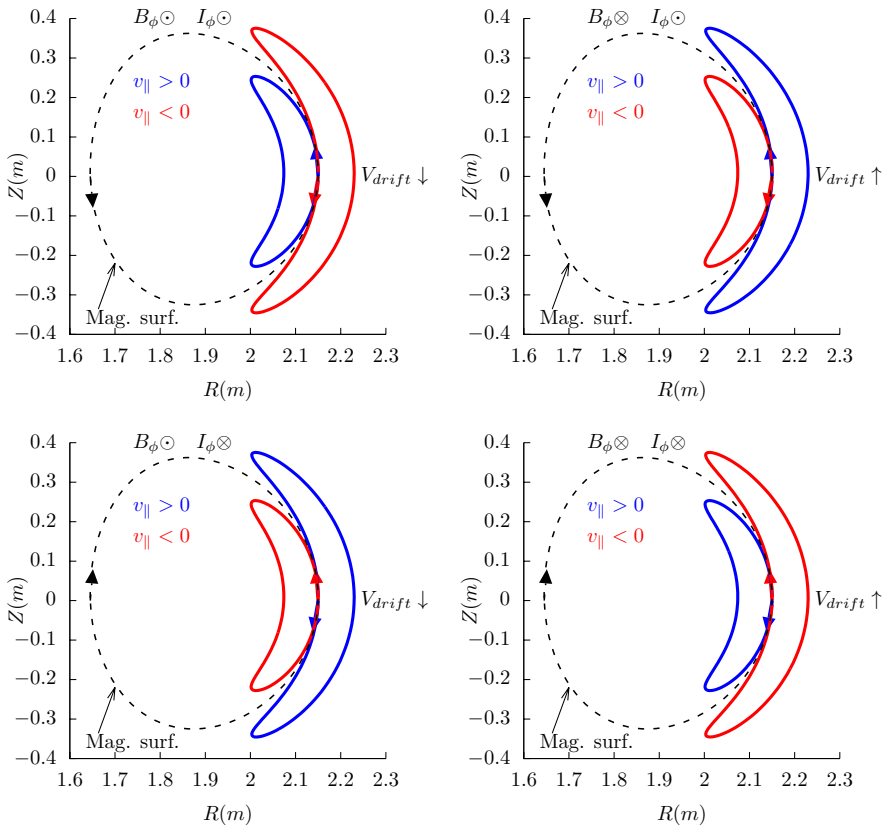

Figure 17. Projection of trapped orbits on the poloidal plane for 4 magnetic configurations. A Deuterium ion of 20keV is launched from the low-field-side midplane ($R_{\text{initial}} = 2.15m$, $Z_{\text{initial}} = 0m$) with pitch angle $\theta = 75°(v_\parallel > 0)$ and $\theta = 105°(v_\parallel < 0)$. Note that $v_\parallel > 0$ implies that the zero-width orbit in the poloidal plane is along the direction of the poloidal magnetic field, which is in turn determined by the direction of the toroidal plasma current. The magnetic equilibrium is from EAST discharge #62585@2.8s (gfile provided by ZhengZheng). The direction of toroidal plasma current, magnetic field, and the corresponding magnetic drift are indicated on the figures.

Figure 17 can be used to identify the direction of the bootstrap current due to the radial density gradient of trapped particles. Examining all the cases in Fig. 17, one finds that the bootstrap current is always along the direction of plasma current, and the bootstrap current direction is independent of the charge sign.

Next, consider passing particles launched from the low-field-side midplane. Figure 18 plots all the 4 possible cases.

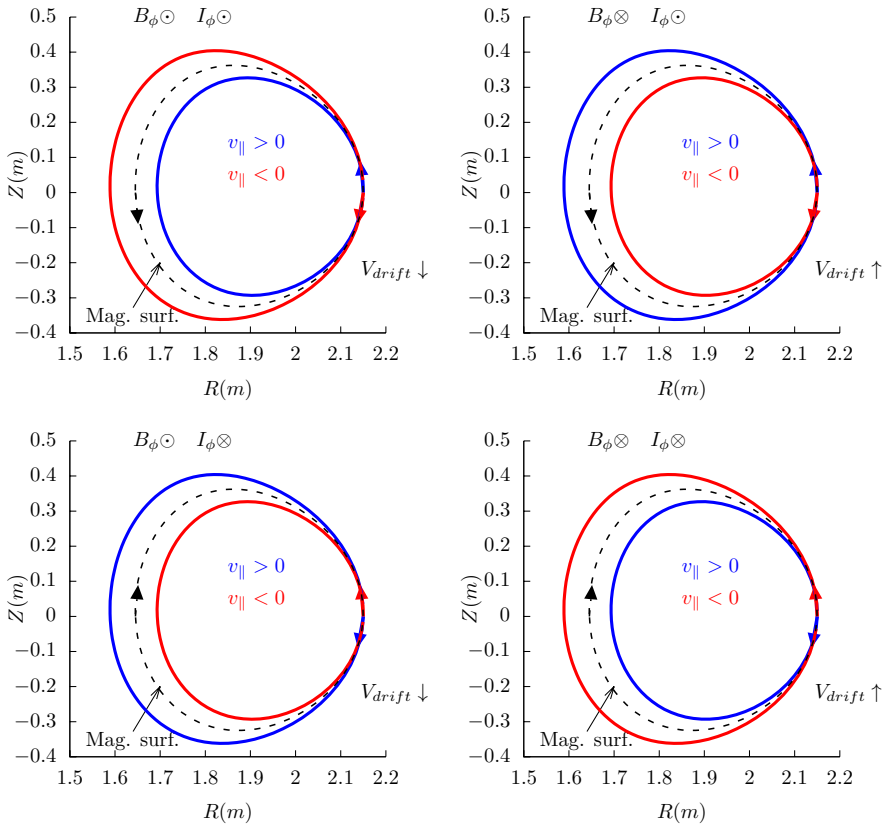

Figure 18. Projection of passing orbits on the poloidal plane for various magnetic configurations. A Deuterium ion of 20keV is launched from the low-field-side midplane ($R_{\rm ini} = 2.15m$, $Z_{\rm ini} = 0m$) with pitch angle $\theta = 50°(v_\parallel > 0)$ and $\theta = 130°(v_\parallel < 0)$. The magnetic equilibrium is from EAST discharge #62585@2.8s (gfile provided by ZhengZheng). The direction of plasma current, magnetic field, and the corresponding magnetic drift are indicated on the figures.

Next, consider a particle launched from the high field side midplane, which must be a passing particle. Figure 19 plots all the 4 possible cases.

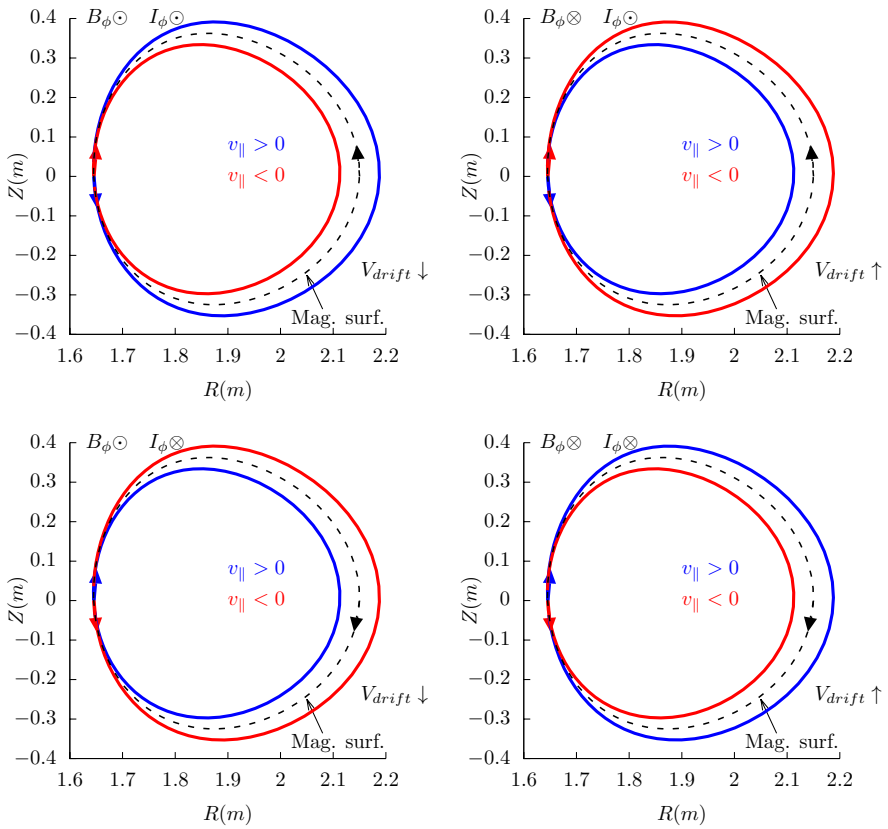

Figure 19. Projection of passing orbits on the poloidal plane for various magnetic configurations. A Deuterium ion of 20keV is launched from the high-field-side midplane ($R_{\rm ini} = 1.6452m$, $Z_{\rm ini} = 0m$) with pitch angle $\theta = 50°(v_\parallel > 0)$ and $\theta = 130°(v_\parallel < 0)$. The magnetic equilibrium is from EAST discharge #62585@2.8s (gfile provided by ZhengZheng). The direction of plasma current, magnetic field, and the corresponding magnetic drift are indicated on the figures.

Examining the above results, one finds that reversing the direction of the toroidal magnetic field does not change the projection of orbits on the poloidal plane, i.e., the location and shape of the poloidal orbits remain the same. However the direction of the poloidal motion is changed from clockwise (anti-clockwise) to anti-clockwise (clockwise). (This is because $v_\parallel$ of a particle changes sign when the toroidal field is reversed and thus the direction of the poloidal motion changes).

Examining the above results, we can also find that, for particles launched from low-field-side midplane, co-current particles have their orbits inside the magnetic surface at which the particle is initially located, and counter-current particles have their orbits outside of the magnetic surface. For particles launched from the high-field-side midplane, the conclusion is reversed, i.e., co-current particles have their orbits outside the magnetic surface where they are initially located, and counter-current particles have their orbits inside of the magnetic surface.

These conclusions have important implications for the neutral beam injection, where orbits outside a reference magnetic surface (birth location) are more likely to be lost to the wall of the machine. If the neutral beam injection (NBI) is along the same direction of the plasma current, it is called the co-current injection. Otherwise it is called the counter-current injection. Using the above conclusions, we know that, for co-current injection, ions ionized at the low-field-side have better confinement compared with those ionized at the high-field-side. For the counter-current injection, ions ionized at the high-field-side have better confinement compared with those ionized at the low-field-side. Whether the overall confinement of ions due to co-current injection is better or worse than that of the counter-current injection depends on the ratio of number of ions deposited at the low-field-side to that deposited at the high-field side. For the shine-

through loss to be small, most neutral must ionize at the low-field-side (most neutrals ionizing at the the high-field side usually means a very high shine-through loss fraction (>50%)). Therefore, with the assumption that most neutral beam particles are ionized on the low-field-side, co-current injection is better than counter-current injection in terms of the first-orbit loss.

Figure 20 and 21 compares the poloidal orbits of energetic Deuterium particles ionized at the low-field-side midplane due to co-current and counter-current injection. The results indicate again that the counter-injected particles ionized at the low-field-side midplane are easy to be lost from the plasma because their orbits are outside the flux surface where they are ionized, and thus are more likely to touch the first wall.

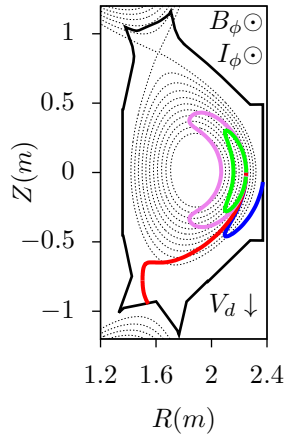

Figure 20. Poloidal orbits of Deuterium particles of 50keV ionized at the low-field-side midplane ($R = 2.25m$, $Z = 0m$) with a birth pitch angle $\theta = 125°$ (red), $\theta = 105°$ (blue), $\theta = 75°$ (green), and $\theta = 65°$ (violet). Pitch angle θ is the included angle between the magnetic field and the velocity of particles. Since the magnetic field and the plasma current are in the same direction for this case, $\theta > 90°$ means counter-current injection and $\theta < 90°$ means co-current injection. The counter-injected particles are easy to be lost from the plasma because their orbits are outside the flux surface where they are ionized, and thus are more likely to touch the first wall. The magnetic equilibrium is for EAST discharge #62585@2.8s, which is a upper single-null configuration (gfile provided by ZhengZheng).

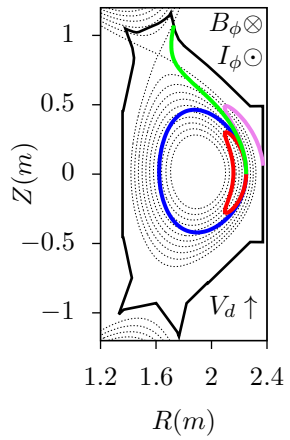

Figure 21. Poloidal orbits of Deuterium particles of 50keV ionized at the low-field-side midplane ($R = 2.25m$, $Z = 0m$) with a birth pitch angle $\theta = 125°$ (blue), $\theta = 105°$ (red), $\theta = 75°$ (violet), and $\theta = 60°$ (green). Since the magnetic field and the plasma current are in the opposite direction for this case, $\theta > 90°$ means co-current injection and $\theta < 90°$ means counter-current injection. The magnetic equilibrium is from EAST discharge #62585@2.8s but with the direction of the toroidal magnetic field reversed.

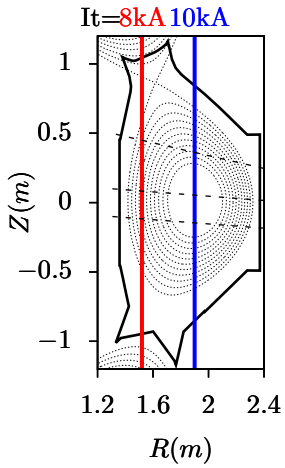

Figure 22. The resonant layer of 50MHz electromagnetic wave with the third harmonic of ${}^1_1H$ ion cyclotron frequency on EAST tokamak. The toroidal magnetic field of EAST is approximately given by $B_\phi = 4.160 \times 10^{-4} I_s / R$, where I_s is the current in a single turn of the TF coils, which in in the range from $8000A$ to $10000A$ for usual EAST discharges. The ion cyclotron angular frequency is given by $\omega_{ci} = B_\varphi e / m_i$. The small Dopper frequency shift $k_\parallel v_\parallel$ is not included in the estimation of the resonant layer.

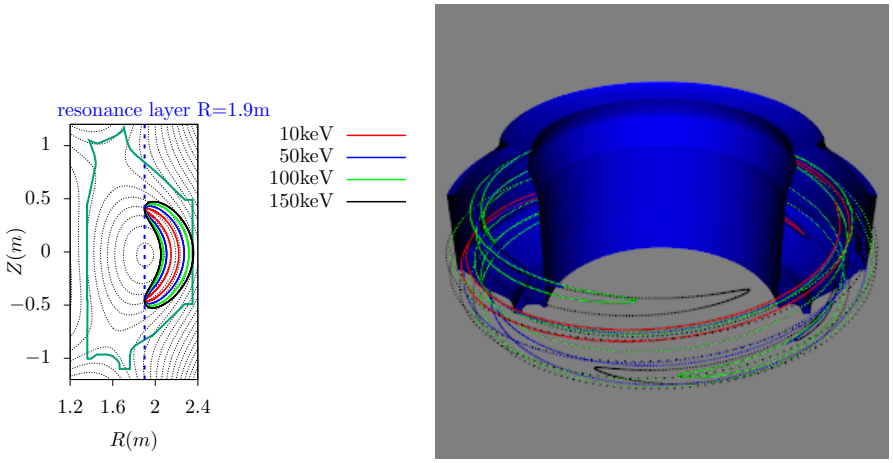

Figure 23. $I_s = 11\text{kA}$, $B_\phi = 4.160 \times 10^{-4} I_s / R$
fundament harmonic of ${}^1_1H$ ion cyclotron frequency, $37\text{MHZ} = \Omega / 2\pi$, where $\Omega = B_\phi e / m$.

5.7 Toroidal procession

Figure 24 plots the guiding centers orbits for particles launched at the low-field-side of the mid-plane with different values of the pitch angle θ.

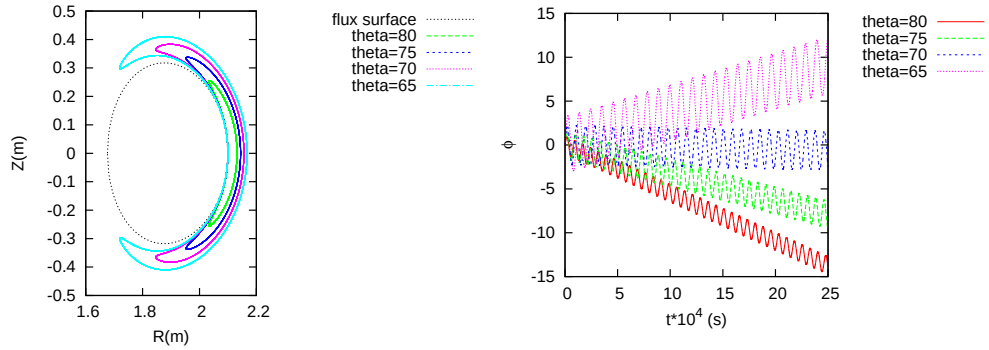

Figure 24. Left: projection of guiding center orbits of trapped particles on (R, Z) plane. Right: Toroidal motion of guiding center of the trapped particles. All particles have the same kinetic energy $\varepsilon = 10$keV and are launched from the low-field side midplane of the reference magnetic surface $(R = 2.1, Z = 0)$. The equilibrium is a Solovev equilibrium with $R_0 = 1.9m$, $B_0 = 2.0$Tesla, $\kappa_0 = 1.5$, $Ze_0 = 1.5$, $g = 3.8$mT.

Figure 24 shows (1) the toroidal procession of deeply trapped particles is faster than that of the shallowly trapped particles and (2) the direction of the toroidal recession of the particle with $\theta = 65^\circ$ is different from the others.

Procession angular frequency of a trapped particles (from Porcelli's slide):

$$\omega_D = \frac{v^2}{2\Omega_c R r} = \frac{E_k}{BZeRr}, \tag{100}$$

where E_k is the kinetic energy of the particle. Equation () indicates that the procession frequency is proportional to the energy of the particle.

$$\omega_D = \frac{v^2}{2\Omega_c R r} = \frac{v^2}{2\overline{B}\Omega_n \overline{R}\,\overline{r} L_n^2} = \Omega_n \frac{\bar{v}^2}{8\pi^2 \overline{B}\,\overline{R}\,\overline{r}} \tag{101}$$

Compared with the results given by the numerical code, the above results seems to be roughly correct when the orbit is not near the magnetic axis.

$$\bar{v}_\perp^2 = \frac{v_\perp^2}{v_n^2} = \frac{2B\mu}{m v_n^2} = \overline{B}\frac{2B_n \mu}{m v_n^2} = 2\overline{B}\overline{\mu} \tag{102}$$

5.8 Radial drift –check!!

$$\frac{d\Psi}{dt} = \mathbf{V}_d \cdot \nabla\Psi = \frac{1}{\Omega}\mathbf{b} \times \left(\frac{\mu}{m}\nabla B + v_\parallel^2 \boldsymbol{\kappa}\right) \cdot \nabla\Psi$$

$$\frac{d\Psi}{dt} = \frac{1}{B\Omega}\mathbf{B} \times \left(\frac{\mu}{m}\nabla B + v_\parallel^2 \boldsymbol{\kappa}\right) \cdot \nabla\Psi$$

$$\frac{d\Psi}{dt} = -\frac{1}{B\Omega}\mathbf{B} \times \nabla\Psi \cdot \left(\frac{\mu}{m}\nabla B + v_\parallel^2 \boldsymbol{\kappa}\right)$$

using

$$\mathbf{B} = \nabla\Psi \times \nabla\phi + g\nabla\phi$$

$$\frac{d\Psi}{dt} = -\frac{1}{B\Omega}(\nabla\Psi \times \nabla\phi \times \nabla\Psi + g\nabla\phi \times \nabla\Psi) \cdot \left(\frac{\mu}{m}\nabla B + v_\parallel^2 \boldsymbol{\kappa}\right) \tag{103}$$

Noting that both ∇B and $\boldsymbol{\kappa}$ are approximately along $-\hat{\mathbf{R}}$ direction, which is perpendicular to $\nabla\phi$, Eq. (103) is written as

$$\frac{d\Psi}{dt} = -\frac{1}{B\Omega}(g\nabla\phi\times\nabla\Psi)\cdot\left(\frac{\mu}{m}\nabla B + v_{\parallel}^2\boldsymbol{\kappa}\right)$$

$$\frac{d\Psi}{dt} = \frac{1}{B\Omega}g\mathbf{B}_p\cdot\left(\frac{\mu}{m}\nabla B + v_{\parallel}^2\boldsymbol{\kappa}\right)$$

if

$$\frac{d\Psi}{dt}(\Psi_{\rm lcfs}-\Psi_{\rm axis})>0,$$

then the drift from the local magnetic surface is outward, otherwise, the drift is inward.

$$\frac{d\Psi}{dt}(\Psi_{\rm lcfs}-\Psi_{\rm axis}) = \frac{1}{B\Omega}g\mathbf{B}_p\cdot(-\hat{\mathbf{R}})(\Psi_{\rm lcfs}-\Psi_{\rm axis})$$

Examining the right-hand side of Eq. (103), we find that $\mathbf{B}_p$ and $(\Psi_{\rm lcfs}-\Psi_{\rm axis})$ change signs simultaneous when the toroidal plasma current I_ϕ change sign, thus the direction of $\mathbf{B}_p(\Psi_{\rm lcfs}-\Psi_{\rm axis})$ is independent of the sign of I_ϕ. Therefore the sign of the radial drift is independent of the sign of I_ϕ.

5.9 Width of guiding center orbit

The gyroradius of a particle is given by $\rho_\alpha = mv/BZe$, which can be further written as

$$\rho_\alpha = \frac{\sqrt{2mE_k}}{BZe}, \tag{104}$$

where E_k is the kinetic energy of the particle. For an electron with the same kinetic energy of a ion, Eq. (104) indicates that the gyroradius of the electron is smaller than that of the ion by the factor $\sqrt{m_e/m_i}$. Now comes the question: Is the width of the guiding center orbit of an electron with the same kinetic energy of a ion smaller than that of the ion? Examine the constant of motion P_ϕ which is given by

$$\frac{P_\phi}{Ze} = \frac{g(\Psi)}{\Omega}v_{\parallel} + \Psi, \tag{105}$$

The function $g(\Psi)/\Omega$ is usually a weak function of Ψ, thus can be assumed to be a constant along a drift orbit. The orbit width can be characterized by $\Delta\Psi$, which is written

$$\Delta\Psi = -g\frac{\Delta v_{\parallel}}{\Omega} = -g\frac{m\Delta v_{\parallel}}{BZe}, \tag{106}$$

where $\Delta v_{\parallel}$ is the variation range of $v_{\parallel}$ in one poloidal period of the orbit. For trapped particles, this variation can be approximated as

$$\Delta v_{\parallel} \approx v_t = \sqrt{\frac{2T}{m}} \tag{107}$$

Using this, Eq. (106) is written as

$$\Delta\Psi = -g\frac{\sqrt{m}\sqrt{2T}}{BZe}, \tag{108}$$

which indicates that, for the same temperature, $\Delta\Psi$ is proportional to $\sqrt{m}$. (For circulating ions, the variation of $v_{\parallel}$ during one poloidal period can not be approximated by v_t. I do not know how to estimate the orbit width in this case).

The variation of the poloidal flux $\Delta\Psi_p$ can be approximated by

$$\Delta\Psi_p = 2\pi R \Delta r B_p \tag{109}$$

where Δr is the variation of the minor radius, B_p is the average poloidal magnetic field on a magnetic surface. Using this and the definition $\Delta\Psi = \Delta\Psi_p/2\pi$ in Eq. (108), we obtain

$$\Delta r = -g\frac{\sqrt{2mT}}{RB_pBZe} \approx -\frac{\sqrt{2mT}}{B_pZe}, \tag{110}$$

which indicates that the width of guiding-center orbits is inversely proportional to the poloidal magnetic field B_p, rather than the toroidal magnetic field B_t (first got to know this conclusion from J. Wesson's book "Science of JET", and later wrote the above derivation).

Comparing Eq. (110) and (104), we know Δr is just the "poloidal Larmor radius" which is obtained by replacing the B in Eq. 104) by the poloidal magnetic field B_p. It follows that the ratio between them is given by

$$\frac{\Delta r}{\rho_i} = \frac{B}{B_p}, \tag{111}$$

which is about q/ε for large aspect-ratio tokamaks, where q is the safety factor.

The average poloidal magnetic field on a magnetic surface near the plasma edge is approximately given by

$$B_p = \frac{\mu_0 I_p}{2\pi a}. \tag{112}$$

Using this, Eq. (110) is written as

$$\Delta r = -\frac{2\pi a\sqrt{2mT}}{\mu_0 I_p Ze}, \tag{113}$$

which indicates that Δr is proportional to $1/I_p$. This explains why high plasma current is beneficial to the confinement of energetic particles (because high current corresponds to smaller orbit width and thus better confinement of energetic particles which usually have larger drift orbit width than thermal particles).

A numerical example in Fig. 25 indicate, as expected, that the guiding center orbit width of an electron with the same kinetic energy of a ion is much smaller than that of the ion.

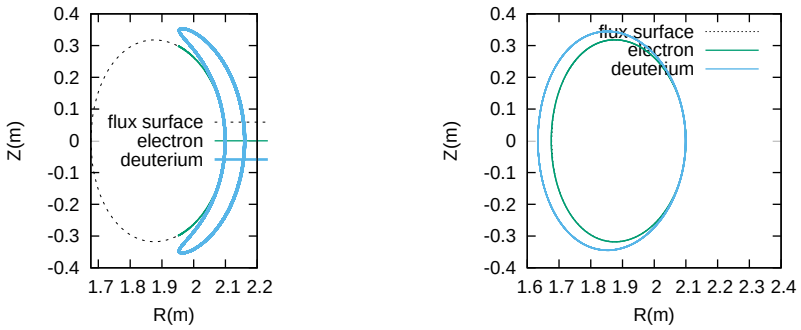

Figure 25. Comparison of the guiding center orbit width of an electron and a Deuteron that have the same value of kinetic energy (20keV). Particles are launched from the low field side of the midplane of the reference flux surface ($R = 2.1m$, $Z = 0.0m$) with pitch angle $\theta = 75°$ (left graph) and $\theta = 55°$ (right graph). The results show that the orbit width of electron is negligibly small (compared with that of the Deuteron) and the orbit almost coincides with the magnetic surface.

5.10 3D trajectory of guiding-center

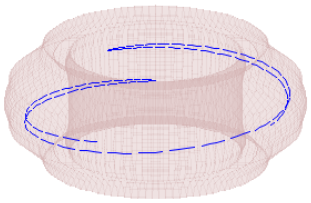

Figure 26. Three-dimensional illustration of the guiding-center orbit of a trapped particle in a tokamak.

6 Numerical results of prompt loss of fast ions

The initial distribution function of fast ions are assumed to take the following form:

$$f(\psi, v, \lambda) = C \exp\left(-\frac{\psi}{\psi_{\text{scale}}}\right) \frac{1}{v^3 + v_{\text{crit}}^3} \frac{1}{2} \text{erfc}\left(\frac{v - v_{\text{birth}}}{\Delta_v}\right) \exp\left(-\frac{(\lambda - \lambda_0)^2}{\Delta_\lambda^2}\right), \tag{114}$$

where the constant C is set to achieve desired stored energy of energetic particles. Figure 27 plots the time evolution of the loss fraction due to the prompt loss (also called first orbit loss) in EAST#48916 at 4.6s.

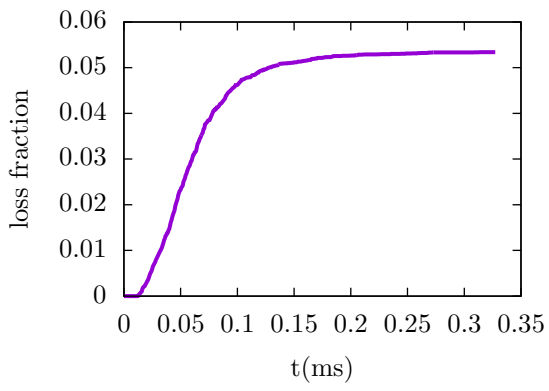

Figure 27. Time evolution of fast ions loss fraction in EAST discharge #48916 at 4.6s. Fast ions distribution function is given by Eq. (114).

$$d\Gamma = dV_s dV_v = R dR dZ d\phi 2\pi \frac{B}{m} dv'_{\parallel} d\mu$$

$$\frac{d\Gamma}{L_n^3 v_n^3} = \overline{R}\ d\ \overline{R}\ d\ \overline{Z}\ d\phi 2\pi \frac{B}{m v_n^2}\ d\overline{v}'_{\parallel} d\mu = \overline{R}\ d\ \overline{R}\ d\ \overline{Z}\ d\phi 2\pi \frac{\overline{B}}{m v_n^2 / B_n}\ d\overline{v}'_{\parallel} d\mu =$$

$$\overline{R}\, d\overline{R}\, d\overline{Z}\, d\phi 2\pi \overline{B}\, d\overline{v}'_{\parallel} d\overline{\mu} \tag{115}$$

Marker's phase-space volume V_j

7 Use constants of motion to determine orbit loss

This section discusses determining the prompt loss of ions by using the constants of motion. This work was motivated by Dr. Chengkang Pan, who shares an office with me and recently (2014) published a NF paper discussing this topic.

7.1 Critical velocity for ions to touch a boundary

There are three constants of motion for a guiding center drift, namely, the canonical toroidal angular momentum P_ϕ, the magnetic moment μ, and the total kinetic energy ε, which are given, respectively, by

$$P_\phi = m\frac{g(\Psi)}{B} v\xi + Ze\Psi, \tag{116}$$

$$\mu = \frac{m}{B} v^2 (1-\xi^2), \tag{117}$$

$$\varepsilon = \frac{1}{2} m v^2, \tag{118}$$

where $g(\Psi) = RB_\phi$, ξ is the cosine of the pitch angle of guiding center velocity (with respect to the local magnetic field), $\Psi = RA_\phi$ with A_ϕ being the toroidal component of the magnetic vector potential, Ze and m are the charge and mass of the ion, respectively.

Next, we use the constraint of the three constants of motion to determine whether an ion with a given initial condition can reach a boundary magnetic surface labeled by Ψ_a. The initial conditions of an ion is denoted with (Ψ_0, B_0, v_0, ξ_0), where Ψ_0 labels the flux surface where the particle is initially located, B_0 is the magnetic field strength at the initial location of the guiding-center, v_0 and ξ_0 are the initial velocity and pitch angle. The conditions of the particle when it reach the boundary flux surface are denoted with (Ψ_a, B_a, v_a, ξ_a). Then the conservation of P_ϕ requires

$$m\frac{g(\Psi_0)}{B_0} v_0\xi_0 + e\Psi_0 = m\frac{g(\Psi_a)}{B_a} v_a\xi_a + e\Psi_a. \tag{119}$$

Using the conservation of the kinetic energy, the above equation is written

$$m v_0 \left(\frac{g(\Psi_0)}{B_0}\xi_0 - \frac{g(\Psi_a)}{B_a}\xi_a \right) = e(\Psi_a - \Psi_0). \tag{120}$$

Using the conservation of μ, we obtain

$$\frac{1-\xi_a^2}{B_a} = \frac{1-\xi_0^2}{B_0}, \tag{121}$$

which can be written

$$\xi_a = \pm\sqrt{1 - \frac{B_a}{B_0}(1-\xi_0^2)}. \tag{122}$$

where we does not distinguish between circulating particles and trapped particles. If a particle is a circulating one, then $v_\parallel$ does not change sign and thus ξ does not change sign either. In this case, equation (122) is written

$$\xi_a = \mathrm{sign}(\xi_0)\sqrt{1 - \frac{B_a}{B_0}(1-\xi_0^2)}. \tag{123}$$

If a particle is a trapped one, then both signs ± in Eq. (122) are possible.

Using Eq. (122), equation (120) is written

$$m v_0 \left[\frac{g(\Psi_0)}{B_0}\xi_0 \mp \frac{g(\Psi_a)}{B_a}\sqrt{1-\frac{B_a}{B_0}(1-\xi_0^2)} \right] = e(\Psi_a - \Psi_0), \tag{124}$$

which can be arranged in the form

$$v_0 = \frac{e(\Psi_a - \Psi_0)}{m}\left(\frac{g(\Psi_0)}{B_0}\xi_0 \mp \frac{g(\Psi_a)}{B_a}\sqrt{1-\frac{B_a}{B_0}(1-\xi_0^2)} \right)^{-1}, \tag{125}$$

Equation (125) gives the velocity v_0 needed for the particle to reach the flux surface Ψ_a. The value of v_0 given by Eq. (125) varies, depending on the value of B_a, i.e., depending on the poloidal location on the boundary magnetic flux surface. By scanning the poloidal location on the boundary flux surface, we can obtain the minimum value of v_0, $v_{0\min}$, which is the minimum velocity for a particle with the initial condition (Ψ_0, B_0, ξ_0) to reach the flux surface Ψ_a.

To evaluate the minimum energy for the ions to be lost, we need choose a specific magnetic configuration. Next, we consider a simple large aspect ratio magnetic configuration.

7.2 Large aspect ratio equilibrium

Define (r, θ, ϕ) coordinates by

$$R(r,\theta) = R_{\text{axis}} + r\cos\theta, \tag{126}$$

$$Z(r,\theta) = r\sin\theta, \tag{127}$$

where (R, ϕ, Z) are the cylindrical coordinates and R_{axis} is a constant. The Jacobian $\mathcal{J}$ of (r, θ, ϕ) coordinates can be calculated using the definition, yielding $\mathcal{J} = -Rr$ (refer to my notes on equilibrium).

In (r, θ) coordinates, the toroidal elliptic operator $\Delta^\star\Psi$ is given by (refer to my notes on equilibrium):

$$\Delta^\star\Psi = \frac{1}{r}\frac{\partial}{\partial r}r\frac{\partial\Psi}{\partial r} + \frac{1}{r^2}\frac{\partial^2\Psi}{\partial\theta^2} - \frac{1}{R_0 + r\cos\theta}\left(\frac{\partial\Psi}{\partial r}\cos\theta - \frac{\partial\Psi}{\partial\theta}\frac{1}{r}\sin\theta \right). \tag{128}$$

Assume that the toroidal current density J_ϕ is given and is uniform distributed, $J_\phi = I/S$, where I is the total current within a boundary magnetic surface, S is the poloidal area enclosed by the boundary magnetic surface Since J_ϕ is given, then the expression $J_\phi = -\frac{1}{\mu_0 R}\Delta^\star\Psi$ can be used as a constraint for Ψ, i.e.,

$$\frac{1}{r}\frac{\partial}{\partial r}r\frac{\partial\Psi}{\partial r} + \frac{1}{r^2}\frac{\partial^2\Psi}{\partial\theta^2} - \frac{1}{R_{\text{axis}} + r\cos\theta}\left(\frac{\partial\Psi}{\partial r}\cos\theta - \frac{\partial\Psi}{\partial\theta}\frac{1}{r}\sin\theta \right) = -\mu_0(R_{\text{axis}} + r\cos\theta)\frac{I}{S}, \tag{129}$$

We consider the region $\varepsilon = r/R_{\text{axis}} \ll 1$ (large aspect ratio regime), and further assume the following orderings

$$R_{\text{axis}}\frac{\partial\Psi}{\partial r} \sim O(\varepsilon^{-1})\Psi, \tag{130}$$

and

$$\frac{\partial\Psi}{\partial\theta} \sim O(\varepsilon^0)\Psi. \tag{131}$$

Then the leading order of Eq. (129) is written as

$$\frac{1}{r}\frac{\partial}{\partial r}r\frac{\partial\Psi}{\partial r} = -\mu_0 R_{\text{axis}}\frac{I}{S}. \tag{132}$$

One solution to the above equation is

$$\Psi = -\frac{\mu_0 I}{4S}R_{\text{axis}}r^2. \tag{133}$$

In the (r,θ,ϕ) coordinates, the gradient of Ψ is written

$$\begin{aligned}\nabla\Psi &= \frac{\partial\Psi}{\partial r}\nabla r+\frac{\partial\Psi}{\partial\theta}\nabla\theta+\frac{\partial\Psi}{\partial\phi}\nabla\phi\\ &= -\frac{\mu_0 I}{2S}R_{\rm axis}r\nabla r\end{aligned}\tag{134}$$

Then the poloidal magnetic field is written as

$$\begin{aligned}\mathbf{B}_p &= \nabla\Psi\times\nabla\phi\\ &= -\frac{\mu_0 I}{2S}R_{\rm axis}r\nabla r\times\nabla\phi\\ &= -\frac{\mu_0 I}{2S}R_{\rm axis}r\left(-\frac{1}{\mathcal{J}}\frac{\partial\mathbf{r}}{\partial\theta}\right).\end{aligned}\tag{135}$$

In terms of the cylindrical coordinate system $(R,\ \phi,\ Z)$ and its unit basis vector $\mathbf{e}_R$ and $\mathbf{e}_Z$, a location vector $\mathbf{r}$ is written as

$$\mathbf{r}=R(r,\theta)\mathbf{e}_R(\phi)+Z(r,\theta)\mathbf{e}_Z,\tag{136}$$

then in (r,θ,ϕ) coordinates, we obtain

$$\begin{aligned}\left.\frac{\partial\mathbf{r}}{\partial\theta}\right|_{r,\phi} &= \frac{\partial R}{\partial\theta}\mathbf{e}_R(\phi)+\frac{\partial Z}{\partial\theta}\mathbf{e}_Z\\ &= -r\sin\theta\mathbf{e}_R(\phi)+r\cos\theta\mathbf{e}_Z\\ &= -r\hat{\mathbf{e}}_\theta,\end{aligned}\tag{137}$$

where $\hat{\mathbf{e}}_\theta=\cos\theta\mathbf{e}_Z-\sin\theta\mathbf{e}_R(\phi)$ is a unit vector. Then Eq. (135) is written as

$$\begin{aligned}\mathbf{B}_p &= -\frac{\mu_0 I}{2S}R_{\rm axis}r\left(\frac{-r\hat{\mathbf{e}}_\theta}{Rr}\right)\\ &= -\frac{\mu_0 I}{2S}\frac{r}{1+\frac{r}{R_{\rm axis}}\cos\theta}\hat{\mathbf{e}}_\theta\end{aligned}\tag{138}$$

The toroidal component of the magnetic field is written

$$B_\phi=\frac{g(\Psi)}{R}=\frac{g(\Psi)}{R_{\rm axis}+r\cos\theta}.\tag{139}$$

Consider the case that $g(\Psi)$ is a constant function, $g(\Psi)=B_{\phi 0}R_{\rm axis}$, then Eq. (139) is written

$$B_\phi=\frac{B_{\phi 0}}{1+\frac{r}{R_{\rm axis}}\cos\theta}\tag{140}$$

I am curious about what the safety factor q looks like for the above flat current density profile. Let us calculate q by using $q=d\Psi_t/d\Psi_p$.

$$d\Psi_t=\oint dr\,B_\phi d\ell_p=dr\,g\oint\frac{r}{R}d\theta\tag{141}$$

$$d\Psi_p=\frac{\mu_0 I}{4S}R_{\rm axis}2r\,dr\tag{142}$$

Then

$$q=\frac{d\Psi_t}{d\Psi_p}=\frac{dr\oint\frac{g}{R}r\,d\theta}{\frac{\mu_0 I}{4S}R_{\rm axis}2r\,dr}=\frac{g\oint\frac{1}{R}d\theta}{\frac{\mu_0 I}{4S}R_{\rm axis}2}=\frac{g}{\frac{\mu_0 I}{2S}R_{\rm axis}^2}\oint\frac{1}{1+\varepsilon\cos\theta}d\theta.\tag{143}$$

Using maxima to perform the above integral, the above expression is written as

$$q=\frac{g}{\frac{\mu_0 I}{2S}R_{\rm axis}^2}\frac{2\pi}{\sqrt{1-\varepsilon^2}}=\frac{4\pi Sg}{\mu_0 IR_{\rm axis}^2}\frac{1}{\sqrt{1-\varepsilon^2}}.\tag{144}$$

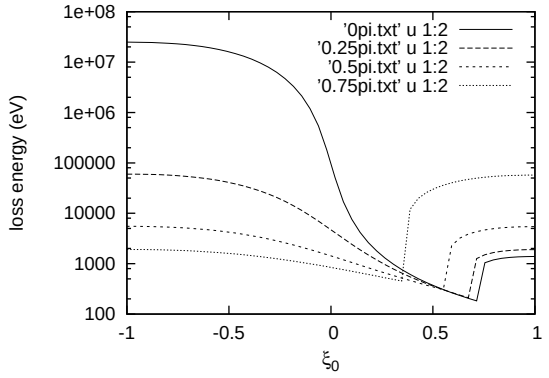

Figure 28. Minimum loss energy as a function of the cosine of the launching pitch angle. $\rho = 0.98$

The minimum value of v_0, denoted with $v_{0\min}$, is reached when $\theta = \pi$ or $\theta = 0$ depends on the $\pm$ in Eq. (168).

$$v_0 = \frac{e}{m R_0}\frac{\mu_0 I}{4\pi a^2}\overline{R}(a^2 - r^2)\left(\xi_0 \mp \mathrm{sign}(\xi_0)\frac{\overline{R}+a}{\overline{R}+r}\sqrt{1-\frac{\overline{R}+r}{\overline{R}+a}(1-\xi_0^2)}\right)^{-1}. \tag{145}$$

$$v_{0\min}(\xi_0) = \max\left(\min\left(v_0(\xi_0,\theta)\right), 0\right) \tag{146}$$

(in practice ψ_a is usually different from the actual poloidal flux Ψ_p and is related to Ψ_p by $\psi_a = \pm|\Psi_p|/2\pi + C$, where C is a constant)

We consider the confinement of the particles. The method is to determine whether the particles can reach a boundary flux surface by making use of the three constants of the motion. The boundary flux surface is labeled by ψ_a, where ψ_a is the poloidal flux within that flux surface.

8 Equations of guiding-center motion—outdated, will be deleted

YJ's remark: This section is outdated because I have found a more accurate form of the equations of the guiding center motion, as given in Sec. 1. Besides to be more accurate, the new form is compact and suitable for numerical implementation

The equations for the guiding center motion are given by (refer to my note "collisionless_drift_kinetic_equation.tm")

$$\dot{\mathbf{X}} = v_\parallel \mathbf{b} + \frac{1}{\Omega}\mathbf{b}\times\left(\frac{\mu}{m}\nabla B + v_\parallel^2 \boldsymbol{\kappa}\right), \tag{147}$$

and

$$\dot{v_\parallel} = -\frac{\mu}{m}\mathbf{b}\cdot\nabla B + v_\parallel \boldsymbol{\kappa}\cdot\dot{\mathbf{X}}, \tag{148}$$

where $\mu \equiv m v_\perp^2 / (2B)$, $\mathbf{b} = \mathbf{B}/B$. The term $v_\parallel \boldsymbol{\kappa}\cdot\dot{\mathbf{X}}$ in Eq. (148) can be further simplified by using Eq. (147), which gives

$$\dot{v_\parallel} = -\frac{\mu}{m}\mathbf{b}\cdot\nabla B + \frac{v_\parallel \mu}{m\Omega}\boldsymbol{\kappa}\cdot\mathbf{b}\times\nabla B \tag{149}$$

where use has been made of that the curvature $\boldsymbol{\kappa}$ is perpendicular to $\mathbf{b}$.

[Benchmark: In GTC simulation (refer to H. Zhang's paper[6]), the time derivative of $v_\parallel$ is given by

$$\dot{v_\parallel} = -\frac{\mathbf{B} + B v_\parallel/\Omega_\alpha \nabla\times\mathbf{b}}{mB}\cdot\mu\nabla B \tag{150}$$

$$\Longrightarrow \dot{v_\parallel} = -\frac{\mu}{m}\mathbf{b}\cdot\nabla B - \frac{v_\parallel\mu}{m\Omega}\nabla\times\mathbf{b}\cdot\nabla B, \tag{151}$$

Next, I prove Eq. (149) is equivalent to Eq. (151). Using $\boldsymbol{\kappa} \equiv \mathbf{b}\cdot\nabla\mathbf{b} = -\mathbf{b}\times\nabla\times\mathbf{b}$, the second term on the right-hand side of Eq. (149) is written as

$$\begin{aligned}
\frac{v_\parallel\mu}{m\Omega}\boldsymbol{\kappa}\cdot\mathbf{b}\times\nabla B &= -\frac{v_\parallel\mu}{m\Omega}(\mathbf{b}\times\nabla\times\mathbf{b})\cdot(\mathbf{b}\times\nabla B) \\
&= -\frac{v_\parallel\mu}{m\Omega}\nabla\times\mathbf{b}\cdot\nabla B + \frac{v_\parallel\mu}{m\Omega}(\mathbf{b}\cdot\nabla B)(\nabla\times\mathbf{b}\cdot\mathbf{b}) \\
&\approx -\frac{v_\parallel\mu}{m\Omega}\nabla\times\mathbf{b}\cdot\nabla B + 0,
\end{aligned} \tag{152}$$

where in obtaining the last equality, use has been made of that $\nabla\times\mathbf{b}\cdot\mathbf{b} \approx 0$ (note that this is correct to the order considered here, I will discuss this later). Using Eq. (152) in Eq. (149) yields

$$\dot{v_\parallel} = -\frac{\mu}{m}\mathbf{b}\cdot\nabla B - \frac{v_\parallel\mu}{m\Omega}\nabla\times\mathbf{b}\cdot\nabla B, \tag{153}$$

which is identical with Eq. (151).]

8.1 Equilibrium magnetic field in tokamak

The tokamak equilibrium magnetic field can be written

$$\mathbf{B} = \nabla\Psi\times\nabla\phi + g(\Psi)\nabla\phi. \tag{154}$$

In my code, the values of the two free functions, $\Psi = \Psi(R, Z)$ and $g(\Psi)$, which specify the magnetic field, is read from the output file "G-eqdsk-file" of EFIT code. Using Eq. (154), the axisymmetric equilibrium magnetic field can be written as

$$B_R = -\frac{1}{R}\frac{\partial\Psi}{\partial Z}, \tag{155}$$

$$B_Z = \frac{1}{R}\frac{\partial\Psi}{\partial R}, \tag{156}$$

$$B_\phi = \frac{g(\Psi)}{R}. \tag{157}$$

The partial derivative of the component of the magnetic field is written as

$$\frac{\partial B_R}{\partial R} = \frac{1}{R^2}\frac{\partial\Psi}{\partial Z} - \frac{1}{R}\frac{\partial^2\Psi}{\partial Z\partial R} \tag{158}$$

$$\frac{\partial B_R}{\partial Z} = -\frac{1}{R}\frac{\partial^2\Psi}{\partial Z^2} \tag{159}$$

$$\frac{\partial B_Z}{\partial R} = -\frac{1}{R^2}\frac{\partial\Psi}{\partial R} + \frac{1}{R}\frac{\partial^2\Psi}{\partial R^2} \tag{160}$$

$$\frac{\partial B_Z}{\partial Z} = \frac{1}{R}\frac{\partial^2\Psi}{\partial R\partial Z} \tag{161}$$

$$\frac{\partial B_\phi}{\partial R} = -\frac{1}{R^2} g(\Psi) + \frac{1}{R} g'(\Psi) \frac{\partial \Psi}{\partial R} \tag{162}$$

$$\frac{\partial B_\phi}{\partial Z} = \frac{1}{R} g'(\Psi) \frac{\partial \Psi}{\partial Z} \tag{163}$$

$$\Rightarrow B = \frac{1}{R} \sqrt{\left(\frac{\partial \Psi}{\partial R} \right)^2 + \left(\frac{\partial \Psi}{\partial Z} \right)^2 + g^2} \tag{164}$$

$$\begin{aligned} \frac{\partial B}{\partial R} &= -\frac{1}{R^2} BR + \frac{1}{R} \frac{1}{2} \frac{1}{BR} \left(2 \frac{\partial \Psi}{\partial R} \frac{\partial^2 \Psi}{\partial R^2} + 2 \frac{\partial \Psi}{\partial Z} \frac{\partial^2 \Psi}{\partial Z \partial R} + 2g \frac{\partial g}{\partial R} \right) \\ &= -\frac{B}{R} + \frac{1}{BR^2} \left(\frac{\partial \Psi}{\partial R} \frac{\partial^2 \Psi}{\partial R^2} + \frac{\partial \Psi}{\partial Z} \frac{\partial^2 \Psi}{\partial Z \partial R} + g \frac{\partial g}{\partial R} \right) \end{aligned} \tag{165}$$

$$\begin{aligned} \frac{\partial B}{\partial Z} &= \frac{1}{R} \frac{1}{2} \frac{1}{BR} \left(2 \frac{\partial \Psi}{\partial R} \frac{\partial^2 \Psi}{\partial R \partial Z} + 2 \frac{\partial \Psi}{\partial Z} \frac{\partial^2 \Psi}{\partial Z^2} + 2g \frac{\partial g}{\partial Z} \right) \\ &= \frac{1}{BR^2} \left(\frac{\partial \Psi}{\partial R} \frac{\partial^2 \Psi}{\partial R \partial Z} + \frac{\partial \Psi}{\partial Z} \frac{\partial^2 \Psi}{\partial Z^2} + g \frac{\partial g}{\partial Z} \right) \end{aligned} \tag{166}$$

In my numerical code, the numerical data of the poloidal flux function $\Psi(R, Z)$ and toroidal field function $g(\Psi)$ are read in from the output G-eqdsk file of the EFIT code. Then all the partial derivatives are calculated by using central finite-difference. The linear interpolation is used to evaluate the various quantities that are needed at the instantaneous location of guiding-centers to push the orbits.

8.1.1 Solovév equilibrium

When I began to write the guiding center orbit code, in order to avoid the numerical interpolating, I use Solovev's analytic equilibrium. (The latest version of my code constructs magnetic field by reading the output G-eqdsk file of the EFIT code and thus can treat general tokamak magnetic field.) The Solovév equilibrium is an analytic equilibrium in which the poloidal flux function Ψ is given by

$$\Psi = \frac{B_0}{2R_0^2 \kappa_0 q_0} \left[R^2 Z^2 + \frac{\kappa_0^2}{4} (R^2 - R_0^2)^2 \right], \tag{167}$$

where B_0, R_0, κ_0, q_0 are constant parameters. Using Eq. (167), the partial derivatives are written as

$$\frac{\partial \Psi}{\partial R} = \frac{B_0}{2R_0^2 \kappa_0 q_0} [2RZ^2 + \kappa_0^2 (R^2 - R_0^2) R], \frac{\partial \Psi}{\partial Z} = \frac{B_0}{R_0^2 \kappa_0 q_0} R^2 Z. \tag{168}$$

$$\frac{\partial^2 \Psi}{\partial R^2} = \frac{B_0}{2R_0^2 \kappa_0 q_0} [2Z^2 + \kappa_0^2 (3R^2 - R_0^2)] \tag{169}$$

$$\frac{\partial^2 \Psi}{\partial Z^2} = \frac{B_0}{R_0^2 \kappa_0 q_0} R^2, \frac{\partial^2 \Psi}{\partial R \partial Z} = \frac{2B_0}{R_0^2 \kappa_0 q_0} RZ \tag{170}$$

$$\tag{171}$$

The toroidal field function g is a constant function, $g = c_g R_0 B_0$, where c_g is a dimensionless constant.

Bibliography

[1] Y. Todo. Properties of energetic-particle continuum modes destabilized by energetic ions with beam-like velocity distributions. *Phys. Plasmas (1994-present)*, 13(8):–, 2006.

[2] John Wesson. *Tokamaks*. Oxford University Press, 2004.
[3] Z. Lin, W. M. Tang, and W. W. Lee. Gyrokinetic particle simulation of neoclassical transport. *Physics of Plasmas*, 2(8):2975, 1995.
[4] Allen H. Boozer. Physics of magnetically confined plasmas. *Rev. Mod. Phys.*, 76:1071–1141, Jan 2005.
[5] Shaojie Wang. Finite bootstrap current density and finite neoclassical reduction of electrical conductivity at the magnetic axis of a tokamak. *Phys. Fluids*, 5(9):3319–3324, 1998.
[6] H. S. Zhang, Z. Lin, I. Holod, X. Wang, Y. Xiao, and W. L. Zhang. Gyrokinetic particle simulation of beta-induced alfvén eigenmode. *Phys. Plasmas*, 17(11):112505, 2010.